FAST METHODS FOR COMPUTING THERMAL-NEUTRON GROUP CONSTANTS IN SINGLE-PIN LATTICE CELLS

R. J. J. STAMM'LER

FAST METHODS FOR COMPUTING THERMAL-NEUTRON GROUP CONSTANTS IN SINGLE-PIN LATTICE CELLS

FAST METHODS FOR COMPUTING THERMAL-NEUTRON GROUP CONSTANTS IN SINGLE-PIN LATTICE CELLS

PROEFSCHRIFT

TER VERKRIJGING VAN DE GRAAD VAN DOCTOR IN DE
TECHNISCHE WETENSCHAPPEN AAN DE TECHNISCHE HOGESCHOOL DELFT
OP GEZAG VAN DE RECTOR MAGNIFICUS
DR. IR. C.J.D.M. VERHAGEN, HOOGLERAAR IN DE AFDELING DER TECHNISCHE NATUURKUNDE,
VOOR EEN COMMISSIE UIT DE SENAAT TE VERDEDIGEN OP
WOENSDAG 4 SEPTEMBER 1968 TE 16 UUR

DOOR

RUDOLF JOHANNES JACOBUS STAMM'LER

NATUURKUNDIG INGENIEUR
GEBOREN TE 'S-GRAVENHAGE

PRINTED IN SWEDEN, 1968, VÄSTRA AROS TRYCKERI AB, VÄSTERÅS

Dit proefschrift is goedgekeurd door de promotor

PROF. DR. J. J. WENT.

The work reported in this thesis was done while the author was with the Reactor Centrum Nederland, the Netherlands. A major part of it is the outcome of the K-7 project, a joint Netherlands-Norwegian project at the Institutt for Atomenergi, Norway.

LIST OF CONTENTS

INTRODUCTION

Many computational schemes that are used for fuel-cycle calculations of heterogeneous thermal reactors superimpose the results of lattice-cell calculations on global or overall reactor-flux calculations. In the global calculations the spatial variation is usually obtained by replacing heterogeneous regions with homogeneous ones of equivalent neutronic properties and applying two- or three-dimensional diffusion theory. The many meshpoints needed in these calculations require a simplified treatment of the energy variable and the range of neutron energies is usually represented by a few groups only. The homogenisation and construction of the few-group constants for the global calculations are only possible when certain properties of the neutron distribution in space and energy in the individual lattice cells are known. This information on the local neutron distribution is provided by the lattice-cell calculations, where the spatial variation as well as the slowing down and thermalisation processes are considered in some detail. Here, as opposed to the global calculations, the local variations are so strong that simple diffusion theory does not suffice and transport theory methods must be used.

It is customary in the lattice-cell calculations to distinguish between epithermal and thermal neutrons. The former have such high energies that the moderating nuclei may be considered as free and at rest. The latter are neutrons which, in the course of slowing down by collisions with moderating nuclei, have acquired such low energies that the chemical binding effects of these nuclei as well as their thermal motion may no longer be neglected. The main problem in the study of epithermal neutrons is the resonance absorption. Outside the resonances, however, the spatial distribution across a cell is practically flat due to the small absorption cross-sections. The study of thermal neutrons poses different and more complicated problems. Firstly, the energy transfer between neutrons and moderator is more complex than for epithermal neutrons, and secondly, the spatial variation of the spectrum across a cell must also be taken into account.

Normally, the thermal neutrons form one of the groups that are used in the few-group scheme of the global calculations. The bulk of the fissions in thermal reactors is caused by these neutrons so that generation of the thermal-group constants is particularly important. Therefore, the study of neutron thermalisation in reactor lattice cells is of fundamental interest for the physics calculations in thermal reactor design.

The great variety of problems consequently met in connection with the fuel-cycle calculations of reactor design covers a major part of the area of static reactor physics.

In principle, each of these problems can be treated in detail and with a high degree of sophistication. To that end many sophisticated codes have been written. They are well suited for interpreting experiments and, hence, for testing the validity of the various physical models and approximations that can be used. However, they are often too time-consuming to be profitable in fuel-cycle studies, where some of the calculations must be carried out thousands of times before an optimum reactor design is reached. Therefore, in contradistinction to sophisticated codes, fast codes must be written with prime emphasis on calculational speed. Of course, the extremely short calculation times which are required can only be achieved at the expense of even cruder approximations. This implies a worsening of the physical description of the problem, which should be investigated by comparison with measurements.

The purpose of this work is to describe and test two fast codes, which have been developed for generating thermal-group constants for single-pin lattice cells moderated by light and/or heavy water. They do not produce the detailed thermal-neutron distribution in space and energy, but rather the average flux and spectrum in the three regions fuel, canning, and moderator. This information is sufficient for constructing the group constants. Experimental verification of these codes is not possible, because the integral quantities they produce cannot be measured directly. Therefore, in order to test their reliability, recourse has been taken to comparison with the more sophisticated code K-7 THERMOS. The latter, in its turn, has been tested against experiments.

It should be pointed out here that the lattice cells considered in this work have been assumed to be surrounded by an infinite array of identical cells so that the cell boundary can be taken as reflective. This implies that the neighbourhood of control elements, burnable poison screens, differently enriched fuel pins, water gaps, etc., cannot be accounted for. As to how far the influence of non-identical surroundings can be felt in the group constants remains a question that needs further investigation. Extensive Monte Carlo calculations or two-dimensional multigroup transport calculations should then be performed on regions that include both the heterogeneity and the nearest pin cells. By comparing their results with those obtained from regular-lattice calculations using different boundary conditions or averaging methods, one may succeed in deriving simple recipes for evaluating thermal-group constants for cells that are in the vicinity of heterogeneities. This falls, however, outside the scope of the present work, which deals with the idealised situation of a regular lattice and, hence, represents only the first step of a reactor lattice homogenisation.

The integral neutron-transport equation, which is the starting point of the computational methods described in this work, is briefly discussed in the first chapter.

In the second chapter the basic physical models of K-7 THERMOS are reviewed. Much of the material presented there is of general interest for thermalisation studies and has also been incorporated in the fast codes. Although K-7 THERMOS is a highly advanced programme, it cannot describe all effects in detail. Even the most elaborate

energy transfer model remains an approximation, while, in the spatial part of the calculations, neither anisotropic scattering nor the actual square or hexagonal shape of the cell is treated exactly. The various approximations that have been used are discussed and expected to be satisfactory.

However, no matter how sophisticated a computational model like K-7 THERMOS may be, the final check of its reliability should be provided by testing it against experimental data. This naturally implies that the experimental data available are accurate, and that all the perturbing effects of the measuring devices have been carefully eliminated. In some of the experimental techniques the perturbations are small enough to justify a crude determination of their magnitude only. In other methods they are larger and require more careful evaluation. However, it seems to have been a rule rather than an exception to underestimate or even neglect these perturbing effects, thereby leaving considerable uncertainties which render a comparison with theoretical results invalid. Therefore, in the third chapter, where K-7 THERMOS is compared with measurements, emphasis has been laid on the different ways in which these perturbations have been evaluated. The satisfactory agreement of K-7 THERMOS with those experiments where the perturbations were carefully determined indicates that its theoretical models are sound and do not introduce serious errors in the lattices studied. The comparison has been confined to cold and unpoisoned uranium lattices, since accurate experimental data on power and plutonium lattices are still lacking. However, if the theoretical models are adequate for the investigated cases one may, within certain limits, apply them also to light- and/or heavy-water-moderated power and plutonium lattices. This is not necessarily true for lattice cells that are in the vicinity of a control element, a water gap, or any other heterogeneity.

In the fourth chapter the fast codes DATAPREP-II and SATAN are described. The former reduces the problem to a one-group calculation of flux ratios using effective cross-sections. These cross-sections are averages over the cell spectrum, which has been assumed spatially to be independent. The latter calculates flux ratios for a number of energy groups and homogenises the cell by flux- and volume-averaging the cross-sections per group. The average cell spectrum is then evaluated from which, using also the energy-dependent flux ratios, the thermal-group constants can be constructed.

In the fifth chapter these codes are extensively tested against K-7 THERMOS. The SATAN results appear to be in good agreement with K-7 THERMOS, while neglecting of the spatial variation of the spectrum turns out to be a serious drawback for DATAPREP-II. The general conclusion is: thermal-group constants for regular single-pin lattices, moderated by light and/or heavy water, can be generated by the fast code SATAN with essentially the same reliability as that of the sophisticated code K-7 THERMOS. This can be advantageously used in the fuel-cycle calculations of power reactor design, where thermal-group constants are of importance and may have to be evaluated thousands of times.

1. THE INTEGRAL NEUTRON TRANSPORT EQUATION

The Boltzmann integro-differential equation provides the most general description of the neutron population in space, energy, and time. In the present study time dependence will not be considered and the energy variable will be limited to the thermalisation range $0 < E < E^*$. Even then, the Boltzmann equation is too unwieldy to be handled numerically and the assumption of isotropic scattering will be introduced so that the angular dependence can be integrated out. This leads to the following neutron transport equation, which will serve as the starting point for the numerical methods to be discussed hereafter.

$$\Sigma_t(\mathbf{r}, E)\,\Phi(\mathbf{r}, E) = \int d\mathbf{r}'\; T(\mathbf{r}' \to \mathbf{r}, E)\left[S(\mathbf{r}', E) + \int_0^{E^*} dE'\,\Sigma_s(\mathbf{r}', E' \to E)\,\Phi(\mathbf{r}', E')\right] \tag{1}$$

where

$\Phi(\mathbf{r}, E)$ = the neutron flux, i.e., the number of neutrons per unit volume of the phase space $(\mathbf{r}, E)$ multiplied by their speed v (throughout this work E will be expressed in eV and the speed in 2200 m/s units);

$\Sigma_t(\mathbf{r}, E)$ = the macroscopic total cross-section, which is the sum of the macroscopic cross-sections for absorption, $\Sigma_a(\mathbf{r}, E)$, and for scattering, $\Sigma_s(\mathbf{r}, E)$;

$S(\mathbf{r}, E)$ = the neutron source at $(\mathbf{r}, E)$ due to slowing down of epithermal neutrons in the thermalisation range;

$T(\mathbf{r}' \to \mathbf{r}, E)$ = the transport kernel for neutrons with energy E, i.e., the contribution to the collision density at $\mathbf{r}$ due to a unit isotropic source at $\mathbf{r}$;

$\Sigma_s(\mathbf{r}, E' \to E)$ = the scattering kernel at $\mathbf{r}$, i.e., the macroscopic cross-section for changing the neutron energy from E' to the unit energy range at E.

In the above equation the scattering kernel is the 0th spherical harmonic moment of the more general kernel $\Sigma_s(\mathbf{r}, E' \to E, \mu)$, where μ is the cosine of the scattering angle in the laboratory system. The higher moments do not occur as a result of the assumption of isotropic scattering. The anisotropy of the kernel can, in principle, be treated by a spherical harmonics technique, which leads to a set of integro-differential equations for the moments of the angular flux $\Phi(\mathbf{r}, E, \Omega)$, where Ω is the unit vector in the direction of motion of the neutrons. However, neither the capacity of the existing scattering models to generate reliable higher moments of the kernel, nor the complexity of the resulting equations warrants a treatment of anisotropy better than to the first order. Because of its involved numerical character such an approach will, in general, only be practicable in combination with a P_1 or, at most, a P_3 transport calculation. Symbolically this will be denoted $P_1 G_1$ and $P_3 G_1$, and the approximation represented by Eq. (1) will then be $P_\infty G_0$. The latter is to be preferred to the $P_3 G_1$ approach because in and near predominantly absorbing media the P_3 approximation cannot treat accurately enough the anisotropy of neutron transport (not to be confused with anisotropy of scattering), and more spherical harmonics would be needed

to describe $\Phi(\mathbf{r}, E)$, i.e., the 0th moment of the angular flux. A $P_\infty G_1$ approach is only feasible in slab geometries, where it was used by Honeck [1] to investigate the first-order anisotropy of scattering. He found that even for more realistic geometries than slab lattices first-order anisotropy could be approximately accounted for by applying the transport correction, i.e., reducing the scattering cross-section by the quantity

$$\overline{\mu}(E)\,\Sigma_s(E) = \int_0^{E^*} \mathrm{d}E' \int_{-1}^{1} \mu \mathrm{d}\mu\, \Sigma_s(E \to E', \mu) \tag{2}$$

Takahashi [2] has confirmed this for cylindrical geometries by comparison with multigroup $P_\infty G_1$ calculations on a series of uranium-water lattices. The agreement of the flux ratios was in all cases better than 1.2 %. The scattering cross-section is related to the kernel as follows:

$$\Sigma_s(\mathbf{r}, E) = \int_0^{E^*} \mathrm{d}E'\, \Sigma_s(\mathbf{r}, E \to E') \tag{3}$$

Observe that the usual upper limit ∞ has been replaced with E^* in consistency with the assumption of no upward scattering past cut-off. Usually E^* is chosen between 0.2–1.0 eV. For interpretation of experiments 0.4 eV is a suitable value, since it coincides with the cadmium cut-off, while in many design schemes 0.625 eV is used.

Furthermore, the scattering kernel—and also the higher moments of the more general kernel—must satisfy the detailed balance condition

$$E\,\mathrm{e}^{-E/T}\,\Sigma_s(\mathbf{r}, E \to E') = E'\mathrm{e}^{-E'/T}\,\Sigma_s(\mathbf{r}, E' \to E) \tag{4}$$

This condition states that the solution of the thermalisation problem in a non-absorbing source-free medium will assume the Maxwellian shape

$$M(E, T) = \frac{E}{T^2}\,\mathrm{e}^{-E/T} \tag{5}$$

There are two important properties of the transport kernel of Eq. (1) which will be used later on. They are:

(*a*) The reciprocity relation

$$\frac{T(\mathbf{r}' \to \mathbf{r}, E)}{\Sigma_t(\mathbf{r}, E)} = \frac{T(\mathbf{r} \to \mathbf{r}', E)}{\Sigma_t(\mathbf{r}', E)} \tag{6}$$

which is physically obvious because the neutron paths are reversible.

(*b*) The fact that the neutrons emitted by the unit source at $\mathbf{r}'$ will anyhow collide somewhere in the system (no leakage has been assumed) is expressed by the relation

$$\int \mathrm{d}\mathbf{r}\, T(\mathbf{r}' \to \mathbf{r}, E) = 1 \tag{7}$$

Another important relation can be derived by integrating Eq. (1) over all **r** and $E \leq E^*$. It states that, in the absence of leakage, the total absorption equals the total source

$$\int \mathrm{d}\mathbf{r} \int_0^{E^*} \mathrm{d}E\, \Sigma_a(\mathbf{r}, E)\, \Phi(\mathbf{r}, E) = \int \mathrm{d}\mathbf{r} \int_0^{E^*} \mathrm{d}E\, S(\mathbf{r}, E) \tag{8}$$

This condition of neutron conservation will prove to be useful in iteration techniques for solving Eq. (1). After each iteration step it will be enforced on the iterate and thereby accelerate the convergence.

The problem of solving Eq. (1) can now be divided into two distinct parts, the first of which deals with finding a satisfactory energy-transfer model for generating the scattering kernel. Once this has been done, the remaining spatial part can be treated in any approximation by transport methods. The source term offers no serious difficulties and the usual assumptions from which it is calculated are the existence of a spatially flat $1/E$ epithermal flux, no upward scattering in the epithermal range, and applicability of the free-gas scattering model. The assumption of the conventional $1/E$ slowing-down flux does not hold in the case of strong epithermal absorption, but fortunately the thermal neutron distribution is to a high degree insensitive to the small deviations from the $1/E$ behaviour. The spatial distribution of the epithermal flux, on the other hand, has been measured on several occasions and is flat within a few per cent. The next chapter describes the main features of the sophisticated code K-7 THERMOS, where advanced energy transfer and transport methods have been combined to solve Eq. (1) in the multishell, multigroup approach. The programme is used for testing the various scattering models and other approximations that have been incorporated in the fast methods described in Chapter 4. At the same time, it has served as the sophisticated code against which the fast codes may be tested.

2. A MULTISHELL, MULTIGROUP SOLUTION OF THE INTEGRAL TRANSPORT EQUATION: THE CODE K-7 THERMOS

2.1. General considerations

The integration over the total space in Eq. (1) can be reduced to the unit cell, provided the surrounding medium has been incorporated through boundary conditions on its outer surface. These conditions will be contained in the transport kernel $T(\mathbf{r}' \to \mathbf{r}, E)$, which, in its most general form, is a function of seven variables. However, for infinite slabs, infinite cylinders and spheres the kernel depends on two spatial and one energy variable only. Therefore, although no true reactor lattice can be built up of cylindrical cells, the square or hexagonal cross-section of the actual unit cell is often replaced by a circular one with equal surface area. This is commonly known as the Wigner-Seitz (WS) cell approximation. The computational methods described in this work have been confined to lattices with cylindrically symmetric fuel elements and the WS cell

concept has been used throughout. In this case the transport kernel is only a function of the three variables r, r' and E, while the spatial integration will be over $2\pi r'\,\mathrm{d}r'$ from 0 to R, where R is the radius of the WS cell. Thus, the problem has been reduced to cylindrically symmetric media. For slab lattices, and also for spherical fuel elements, methods similar to those reported below can be applied, but this is of less practical interest and falls outside the scope of the present study.

Before the numerical solution of Eq. (1) is sought, the energy variable will be replaced by the speed, because the scattering kernel is a smoother function of v than of E. Here it is worth noting that the following relations have to be observed whenever a transformation is made from energy to speed variables and vice versa:

$$E = 0.0253\, v^2 \tag{9 a}$$

$$N(v) = 0.0506\, \Phi(E) \tag{9 b}$$

$$S(v) = 0.0506\, v S(E) \tag{9 c}$$

$$\Sigma_s(v' \to v) = 0.0506\, v\, \Sigma_s(E' \to E) \tag{9 d}$$

so that, for example, finding the flux $\Phi(E)$ is equivalent to finding the neutron density $N(v)$.

In order to solve Eq. (1) in the multishell, multigroup approach, the radius of the WS cell and the thermalisation range $0 - v^*$ will be divided into Q intervals and K groups of arbitrary widths Δr_p and Δv_j, respectively. Their mid-points r_p and v_j are assumed to be representative. Eq. (1) then takes the form

$$\Sigma_{qk} N_{qk} = \sum_{p=1}^{Q} T_{pqk} \left(S_{pk} + \sum_{j=1}^{K} P_{pjk} N_{pj} \right) \tag{10}$$

where p and q are spatial indices, while j and k refer to the speed, Σ_{qk} is the total macroscopic cross-section at (r_q, v_k) and N_{qk} the neutron density $N(r_q, v_k)$. Moreover, the source is denoted by

$$S_{pk} = S(r_p, v_k)/v_k \tag{10 a}$$

the scattering matrix by

$$P_{pjk} = \Sigma_s(r_p, v_j \to v_k)\, v_j \Delta v_j / v_k \tag{10 b}$$

and the transport matrix by

$$T_{pqk} = T(r_p \to r_q, v_k)\, \Delta V_p \tag{10 c}$$

where ΔV_p is the volume of the pth cylindrical shell $2\pi r_p \Delta r_p$.

Thus, the integral equation has been transformed into a set of $Q \cdot K$ linear equations. These are solved by an iteration method that employs a Gauss-Seidel technique combined with normalisation and over-relaxation. This method has proved to converge

in all practical cases, while it seldom needs more than 20 iterations to obtain a relative accuracy of better than 10^{-4} in each of the N_{qk} residues. It has been described by the author elsewhere [3].

The code K-7 THERMOS has been developed by the author [3–5]. It evaluates the thermal neutron distribution $N(r, v)$ according to the method outlined above and, although the basic physical principles are due to Honeck [6], this code has been developed independently from his THERMOS [7]. Up to 24 space points and 16 speed groups are allowed with a maximum cut-off of 0.911 eV, while only H_2O, D_2O, oxygen, and graphite can be treated as moderators and at most six different moderating regions are accepted. Furthermore, the code is provided with a cross-section library on magnetic tape from which the cross-section values for each individual case are taken by linear interpolation [4, 5]. The input data per case, like problem size, region data, speed mesh, and compositions, have to be specified as described by the author [4]. A number of options have been included: the user may choose what boundary condition is to be used, whether the transport correction shall be applied or not, whether the source will be computed by the code or read in, and what energy-transfer model must be taken for H or D.

The code has been written in FORTRAN 3600 for the CDC 3600 of the Kjeller Computer Installation, Norway, and has been translated into FORTRAN IV for the GE-625 at ASEA, Västerås, Sweden. The ALGOL versions for the GIER computers in Halden (Norway) and Swierk (Poland) are its direct descendants. MICROFLUX [8] is a similar—independent—code written in ALGOL for the El X-8 computer at RCN, Petten, the Netherlands. The FORTRAN 3600 version is available from the ENEA Computer Programme Library where it has been filed as programme E004.

The code K-7 THERMOS has been described in detail elsewhere [3–5] and even though it differs in many points from Honeck's THERMOS [7], it is not the intention to discuss these differences, which are mainly of a numerical or organisatory character. Both codes have also been the subject of critical investigations concerning their reliability [1, 2, 5, 28, 29, 32]. The remainder of this chapter will be devoted to such an investigation and will therefore contain partly material and conclusions that have already been published. However, the material presented here has been selected and it mainly deals with those assumptions and approximations which are basic both to K-7 THERMOS and to the fast thermalisation codes of Chapter 4. Since a rather large range of lattice types has been included, it is probably the most exhaustive investigation of its kind. At the same time it may serve as a concise description of the principal features of K-7 THERMOS and it will thereby also give an indication of the reliability of this code.

2.2. *The energy-transfer models*

The simplest, and historically the oldest, model that describes the energy transfer between neutrons and moderator is the free-gas model. It considers the moderator nuclei

as free particles of a monoatomic gas with temperature T. The expression for the free-gas scattering kernel was first derived by Wigner and Wilkins, who studied neutron thermalisation in an infinite homogeneous medium [9]. They showed that in case of mass one (hydrogen gas) the kernel greatly simplifies, and that the corresponding integral equation can be transformed into a differential equation. This limiting case of the free-gas model is commonly known as the Wigner-Wilkins (WW) model and it forms the basis of the well-known SOFOCATE code [10]. In the fast code DATAPREP-II, which will be described in Chapter 4, application of the WW model is optional, although there the integral formulation of the problem has been preserved, rather than transforming it into the differential one.

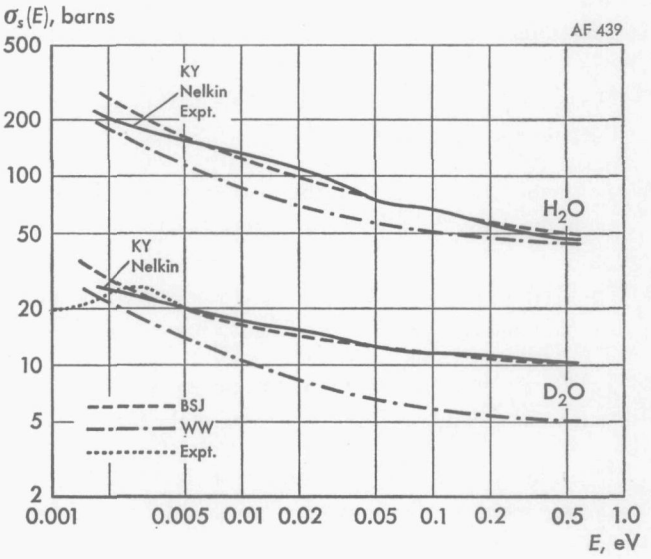

Fig. 1. Scattering cross-sections from different models.

There are, however, two serious drawbacks of the free-gas model. Its main assumption that the moderator nuclei may be considered as monoatomic gas particles is not adequate. The neutrons do not collide with individual nuclei but rather with atoms bounded in molecules (H_2O, D_2O) or with the atoms as part of a crystal lattice (C, BeO). At thermal energies these binding effects may no longer be neglected and they significantly complicate the physical description of the problem. Furthermore, the free-gas model is not capable of reproducing the experimental scattering cross-section (see Fig. 1).

Brown and St. John (BSJ) have proposed two improvements of the free-gas model [12]. The first is the introduction of an effective rotational mass for the protons and deuterons bound in light and heavy water. This approximately accounts for the chemical binding. The effective mass is calculated under the assumption that the

molecule may be treated as a rigid rotator, i.e., the neutron energy must be small compared with the vibrational quanta, but large compared with the differences between the rotational levels of the molecule. It is then defined as the reciprocal of the average of the three eigenvalues of the inverse mass tensor, which can be ascribed to the freely moving mass point representing the bound proton or deuteron ([5], p. 16). The second improvement is of an empirical character. It aims at a better reproduction of the measured cross-section $\sigma_s(E)$. Instead of the assumption of a constant scattering cross-section in the centre of mass system, the following variation of it as a function of the relative speed v_r is assumed:

$$\sigma_s(v_r) = \sigma_0 + B\, e^{-Kv_r^2} \tag{11}$$

where σ_0 is the high energy limit of the cross-section, while B and K are parameters adjustable to fit the experimental data [46]. Detailed formulae and a discussion of the numerical methods used to evaluate the BSJ kernel are given elsewhere [5]. The BSJ model is optional in K-7 THERMOS as well as in the two fast codes to be described in Chapter 4.

A further refinement of the scattering model considers the entire molecule, rather than the individual scattering atom, as the basic dynamical unit. Translation of the molecule as a whole, as well as rotations and vibrations of its nuclei about their equilibrium positions have to be considered. The molecular model for water proposed by Nelkin [13] has found wide use in reactor work. Its basic assumptions are:

(*a*) The translation of the molecule is free and described by the centre of mass motion with weight $\lambda_t = 1/m_0$, where m_0 is the mass of the molecule.

(*b*) The rotation of the molecule is hindered by neighbouring water molecules and the hindered rotation has been replaced by a single oscillator with energy $\omega_r = 0.06$ eV and weight $\lambda_r = 1/m_r$. Here m_r is the effective rotational mass which has been calculated in a slightly different way than in the BSJ model (2.32 instead of 1.884).

(*c*) The three degrees of freedom of the OH bond have been described by isotropic vibrational modes of energies $\omega_1 = 0.205$ eV, $\omega_2 = \omega_3 = 0.481$ eV with equal weights $\lambda_1 = \lambda_2 = \lambda_3$. Here $\lambda_i = 1/m_i$, where m_i is the vibrational mass of the ith mode. Their values have been obtained from the condition that for large energy transfer the free-gas scattering kernel obtains so that $\lambda_1 = \lambda_2 = \lambda_3 = 0.1712$.

An improvement of the Nelkin model has been introduced by Koppel and Young [14], which will be called the KY model. It is an attempt to treat the anisotropy of the vibrational modes of motion of the bound proton kernel, in contrast to the isotropic treatment, which is implicit in the Nelkin model. The hindered rotational weight as well as the vibrational weights will depend on the orientations of the vibrations in the molecule. Koppel and Young approximated the anisotropy by assuming the two-dimensional oscillations of the proton in the bending and torsional modes to be

isotropic in the plane perpendicular to the OH bond (the mass of the oxygen was taken as infinite); the one-dimensional vibrations of the stretching modes were treated exactly. In this case the weights λ_r, λ_1, λ_2 and λ_3 can be written as functions of ν, the cosine of the angle between the OH bond and the momentum transfer vector.

The computer programmes GAKER-KIRA and GAKER-ASEA, written for the CDC 3600 in Kjeller (Norway) and the GE-625 at ASEA (Västerås, Sweden) contain both the Nelkin and the KY model. The former is a special case of the latter where for λ_r, λ_1, λ_2 and λ_3 the average values over ν are used. Detailed formulae and a discussion of the numerical methods used to evaluate these kernels are to be found in an IAEA Report ([5], Chapter II.2).

GAKER-KIRA is available from the ENEA Computer Programme Library as programme E005, written in FORTRAN 3600. K-7 THERMOS contains both models as options, while in the present version of the fast code SATAN use of the KY kernel is optional. These models can also be applied to the scattering of neutrons on heavy water by a suitable choice of the constants [15].

For a comparison of the different models the following integral quantities, which can be derived from the scattering kernel, will be used: the scattering cross-section $\sigma_s(E)$ which is related to the kernel by Eq. (3), and the second Maxwellian moment of energy transfer

$$M_2 = \frac{1}{T^2} \int_0^\infty \mathrm{d}E \int_0^\infty \mathrm{d}E'\, M(E,T)\, \sigma_s(E \to E')(E - E')^2 \tag{12}$$

where $M(E,T)$ is the Maxwellian distribution Eq. (5). Since the 0th moment is simply the Maxwellian averaged cross-section and the first moment vanishes owing to the detailed balance condition Eq. (4), M_2 will be the first of the moments that describes the energy-transfer properties of a given kernel ([5], pp. 9–11).

Concerning $\sigma_s(E)$, all models approach in the high energy limit the true value σ_0 owing to the choice of their constants, while in the low energy limit they reproduce the correct $1/v$ behaviour of the cross-section [5]. From Fig. 1 it follows, however, that the WW model gives a too low value for $\sigma_s(E)$ in the thermalisation range. The BSJ, Nelkin, and KY models, on the other hand, all give good results for $\sigma_s(E)$, except at very low energies, where the scattering cross-section from the BSJ model assumes too early the $1/v$ behaviour and rises too steeply. This does not represent a serious drawback for the BSJ model, because at these low energies (below 0.007 eV) the intensity of the neutron spectrum rapidly falls off and the overall results will be rather insensitive to errors in the scattering kernel in this range.

The thermalising properties of the models can be expressed, to the first order, in terms of the second moment M_2 according to Eq. (12), while the ratio of the second to the 0th moment will describe the mean square energy loss per collision. These values are collected in Table 1 for the three moderators that will be considered in this

work: H_2O, D_2O, and O. In the Nelkin and KY models for H_2O and D_2O the contribution from oxygen was calculated by treating it in the free gas approximation.

It is obvious that in the WW model, where the scattering nuclei have the lowest mass (unity), the energy loss per collision is greatest and the same for all moderators. This does not necessarily result in the softest spectrum, because the too low scattering cross-section (M_0) counteracts this effect. Therefore, the WW model has initially been rather successful for calculating spectra in homogenised water-moderated reactors. The model has also been extended to heavier moderators than H_2O by replacing σ_0 with $\xi\sigma_0$, where ξ is the mean logarithmic energy decrease per collision in the epithermal range. In this way the ratio $\Sigma_a/\xi\Sigma_0$, which is a more essential parameter in thermalisation theory than the mass [16], keeps its correct value. For D_2O this approach approximately preserves the second moment, though at the cost of a scattering cross-section (M_0) which is even lower than that predicted by the free-gas (true mass) model. For heavier moderators M_2 (WW) increasingly deviates from its free-gas value. According to Schofield [17] the latter can be expressed in terms of σ_0 and the mass as follows:

$$M_2(\mathrm{FG}) = \frac{8\,\sigma_0}{m}\left(\frac{m}{1+m}\right)^{3/2} \tag{13}$$

For increasing mass this passes into the heavy free-gas limit $4\,\xi\sigma_0$. The second moment according to the WW model is $2\sqrt{2}\,\xi\sigma_0$, which means that this model gives a too low M_2-value, especially for heavy particles (see also Table 1). The main drawback of the WW model, however, is the strongly underestimated M_0-value. This leads to unacceptable errors in cell calculations, where transport effects are at least as important as the energy transfer. Therefore the WW and the free-gas models which predict too low cross-sections cannot be applied directly. In DATAPREP-II, where the WW model is optional, it is only used to find the spectrum in the homogenised cell. In the transport part of its calculations the experimental values of $\sigma_s(E)$ are then used, averaged over the WW spectrum.

This procedure of using a given model for generating the spectrum but replacing its scattering cross-section by the experimental value is not satisfactory. In a full multishell, multigroup calculation, like in K-7 THERMOS, it is not at all applicable, since

Model	H_2O ($\sigma_0 = 46.1$ *b*)			D_2O ($\sigma_0 = 10.1$ *b*)			O ($\sigma_0 = 3.7$ *b*)		
	M_0	M_2	M_2/M_0	M_0	M_2	M_2/M_0	M_0	M_2	M_2/M_0
WW	60.6	121.3	2.000	7.17	14.33	2.000	0.63	1.27	2.000
Free gas	63.8	121.7	1.908	—	15.57	—	3.81	1.69	0.444
BSJ	92.2	145.1	1.574	13.73	14.52	1.058	—	—	—
Nelkin	93.4	101.9	1.091	13.85	12.22	0.882	—	—	—
KY	95.0	95.1	1.001	13.93	11.66	0.837	—	—	—

Table 1. Integral properties of some scattering kernels.

it would be in conflict with Eq. (3) and thereby make the neutron conservation condition Eq. (8) invalid. The BSJ model does not suffer from a too low $\sigma_s(E)$-value. However, it follows from Table 1 that its second moment M_2 and the ratio M_2/M_0 are too large compared with the values from the more realistic molecular models. It will therefore generate a too soft spectrum. Moreover, the BSJ model, as well as the WW model (except for H_2O), has the disadvantage that it does not pass into the free-gas model with increasing energy, because its effective mass remains constant instead of approaching the true mass. Of the two molecular models, that due to KY produces the hardest spectrum. Since it has been shown that, in the case of heavily $1/v$-poisoned media, even the Nelkin model gives too soft spectra [18], the KY model must be preferred whenever spectral effects are of importance as, for example, in densely packed lattices. In well-thermalised media the spectrum is less sensitive to details of the scattering kernel because, by virtue of the detailed balance condition (4), it will anyhow be close to the Maxwellian distribution Eq. (5).

2.3. *The transport kernel*

The transport kernel T_{pqk} of Eq. (10 c) is the collision density in the qth cylindrical shell owing to an isotropic source of strength ΔV_p placed at the mean radius r_p of the pth shell. A first-flight collision probability technique has been used to evaluate this collision density. The source neutrons emitted at r_p with speed v_k are followed on their way through the WS cell and whenever they reach its outer boundary they are reflected back into the cell. Between two such reflections the neutron trajectory passes through all shells q with $r_q \geq r_p$ and, depending on the direction of emission, through none, some, or even all the other shells too. During each passage through the qth shell a fraction of them collides which, when divided by the volume of that shell ΔV_q, gives a contribution to the collision density there. These contributions are integrated over all emission angles and summed over all the passages to yield the required collision density T_{pqk}. In K-7 THERMOS the integration over the azimuthal angle φ, which can be reduced to the interval from 0 to $\pi/2$, is done by a 10-point Gaussian quadrature [3]. In the one-group version of this code, K-7 TRANSPO (available from the ENEA Computer Programme Library as programme E077), the integration over φ is done by trapezoidal integration with repeated halving of the intervals until an accuracy of 1 per cent is attained [19]. The first method is usually faster, while the second has the advantage of a guaranteed accuracy of better than 1 per cent for all elements T_{pqk}.

The integration over the polar angles leads, in the case of infinitely long cells, to the Bickley functions $Ki_2(x)$, where x is the horizontal projection of the optical distance measured along the trajectory of the neutron. The elements T_{pqk} can then be expressed in terms of differences between two Ki_2 functions. When their arguments are close together, this reduces to Honeck's [6] original approximation

$$Ki_2(x) - Ki_2(x + \Delta x) \approx \Delta x \, Ki_1\left(x + \tfrac{1}{2}\Delta x\right) \tag{14}$$

where Δx is the optical thickness of the horizontally projected path through a given shell. This approximation has only been used when $\Delta x < 0.01$. It means in fact that the shell in which the collision density is calculated—the qth shell—is also represented by its mid-point. This may be a crude approximation when shells with a thickness of more than 0.2 mean free paths are considered.

The heart of the calculation of the transport matrix is the computation of the Bickley functions Ki_1 and Ki_2. They are defined by

$$Ki_n(x) = \int_0^{\pi/2} \mathrm{d}\theta \cos^{n-1}\theta \, \mathrm{e}^{-x/\cos\theta} \tag{15}$$

A possible method would be to read large tables of these functions into the computer and use a fast table lookup with linear interpolation. Tables of $Ki_1(x)$ and $Ki_2(x)$ in the range $0 \leq x \leq 4.99$ are given in a Kjeller Report [3]. Since K-7 THERMOS was originally written for a small computer, another method was chosen. The Bickley functions were expanded in Chebyshev series so that only a compact table of the expansion coefficients was needed from which the wanted function values could be computed [20].

Because not all neutron trajectories starting from r_p will pass through the shells q with $r_q < r_p$, a direct evaluation of T_{pqk} would be insufficiently accurate. The reciprocity relation (6) has therefore been used to evaluate them for these shells from T_{qpk}.

Relation (7) has been enforced upon the transport kernel by multiplying, for fixed p and k, of all elements T_{pqk} by the proper constant. This constant will usually lie close to 1.003, because the source neutrons have been followed on their way through the cell until 0.3 per cent of them were left.

Normally, Eq. (7) should hold rigorously, but representing of the source shells by their mid-points and then applying of the reciprocity relation will reveal to some extent the failure of this shell representation in a deviation of these constants from 1.003. This approximation will increase the diagonal elements T_{ppk} and reduce the others, thus diminishing the neutron transport across the cell. That this may lead to serious errors in complex lattices, when a thick shell is followed by a thin one, has already been shown ([5], Chapter IV.2.1) for a multi-tube fuel element. A better method for evaluating the transport matrix, where this approximation is avoided, has been used by Carlvik [21]. In his method thicker shells may be used and the accuracy is determined by the validity of the flat flux approximation in the individual shells. However, the shell representation of K-7 THERMOS is of no importance for the single-pin lattices studied in this work.

The boundary condition of perfect reflection is inherent in the transport matrix found in this way. For small WS cells, however, this leads to gross overestimates of the moderator-to-fuel flux ratio, as was shown by Newmarch [22]. A better condition

is that of isotropic flux return. It can be easily included in the kernel without its calculational procedure being changed by means of the following stratagem due to Honeck [23]: Add a non-absorbing layer with a thickness of 2.5 mean free paths with an infinitely heavy scatterer to the original WS cell and apply the reflective condition at its outer boundary. Any neutron entering this layer will almost certainly undergo isotropic scattering without energy change. The returning neutron has consequently the desired angular and speed distribution. This extra layer may be represented by a single shell.

For further details of the evaluation of the transport kernel reference should be made to an IAEA Report [5].

2.4. Discussion of the various approximations

The main assumptions of K-7 THERMOS, which are also basic to the fast codes to be described later, can be divided into two classes. On the part of the spatial calculations there are the assumption of isotropic scattering and the WS cell concept. The spectrum calculations, on the other hand, are largely determined by the choice of the energy-transfer model, i.e., by the approximations that are inherent in the scattering kernel. These assumptions will be discussed below.

(*a*) The assumption of isotropic scattering has already been mentioned in Chapter 1. Investigations of Honeck [1] and Takahashi [2] have shown that application of the transport correction accounts for most of the first-order anisotropy of scattering. In one-group calculations this correction is straightforward; the scattering cross-section is reduced by $\overline{\mu}\Sigma_s$. In multigroup calculations it is not so obvious how to apply this correction. Probably the best one can do is to subtract the quantity $\overline{\mu}(E)\,\Sigma_s(E)$ of Eq. (2) from the diagonal elements of the scattering matrix [1] so that the latter integrates properly to the transport cross-section, retaining at the same time the correct energy transfer by not changing the off-diagonal elements. Whenever this leads to negative diagonal elements they are put equal to zero, because otherwise the iteration process for solving Eqs. (10) will not always converge. Normally, when 12–15 speed groups are used, only the three or four highest elements will get negative values. It is clear that an unlimited refining of the speed mesh would result in zero (= negative) diagonal elements everywhere, thus making the transport correction ineffective. Still this is an important correction, as can be seen from Table 2, and one would lose more than would be gained by increasing the number of speed groups beyond a certain limit. Usually, 10-group calculations give approximately the same spectrum as 15-group calculations. It therefore seems to be fully justified to restrict K-7 THERMOS to a maximum of 16 groups.

In the Nelkin and KY models, $\overline{\mu}(E)$ can be evaluated from the expression for $\Sigma_s(E \to E', \mu)$. The BSJ and WW models, however, produce directly $\Sigma_s(E \to E')$, i.e.,

the cosine of the scattering angle has already been integrated out. Whenever these two models were used, the energy dependence of $\overline{\mu}$ was calculated from the effective—energy-dependent—mass which can be determined, according to Radkowsky's pre-

Quantity[a]	Approximation[b]	Lattice[c]									
		1	2	3	4	5	6	7	8	9	10
δ_2	Standard	*1.095*	*1.100*	*1.133*	*1.136*	*1.137*	*1.129*	*1.136*	*1.143*	*1.198*	*1.220*
	No trpt. corr.	−0.1	−0.2	−0.3	−0.3	−0.2	−0.2	−0.2	−0.2	−0.1	−0.1
	Nelkin model	+0.1	0.0	+0.2	+0.2	+0.1	+0.2	+0.2	+0.2	+0.1	0.0
	BSJ model	+0.4	+0.2	+0.6	+0.4	+0.4	+0.3	+0.7	+0.5	+0.2	+0.1
δ_3	Standard	*1.269*	*1.376*	*1.330*	*1.418*	*1.487*	*1.392*	*1.215*	*1.275*	*1.449*	*1.657*
	No trpt. corr.	+0.9	+2.0	+1.3	+2.5	+3.4	+2.4	+0.2	+0.9	+0.9	+1.8
	Nelkin model	+0.1	0.0	+0.2	+0.1	0.0	+0.1	+0.3	+0.2	+0.2	−0.1
	BSJ model	+0.7	+0.1	+1.0	+0.6	+0.4	+0.5	+1.0	+0.8	+0.5	+0.2
ζ_2	Standard	*1.130*	*1.131*	*1.183*	*1.182*	*1.182*	*1.171*	*1.191*	*1.196*	*1.266*	*1.286*
	No trpt. corr.	−0.2	−0.1	−0.3	−0.2	−0.2	−0.2	−0.2	−0.2	−0.1	−0.1
	Nelkin model	+0.1	+0.1	+0.2	+0.2	+0.1	+0.1	+0.3	+0.2	+0.1	0.0
	BSJ model	+0.4	+0.3	+0.7	+0.6	+0.5	+0.4	+0.9	+0.6	+0.3	+0.1
ζ_3	Standard	*1.374*	*1.502*	*1.466*	*1.577*	*1.661*	*1.536*	*1.306*	*1.384*	*1.603*	*1.840*
	No trpt. corr.	+1.0	+2.1	+1.4	+2.7	+3.5	+2.6	+0.3	+1.1	+0.9	+1.9
	Nelkin model	+0.1	−0.1	+0.2	0.0	−0.2	−0.1	+0.4	+0.1	+0.1	0.0
	BSJ model	+0.7	−0.1	+1.0	+0.4	−0.1	+0.2	+1.5	+0.9	+0.6	+0.1
$\overline{v}_1$	Standard	*1.428*	*1.317*	*1.501*	*1.409*	*1.371*	*1.470*	*1.606*	*1.440*	*1.446*	*1.295*
	No trpt. corr.	0.0	0.0	−0.1	−0.1	0.0	0.0	0.0	0.0	−0.1	−0.1
	Nelkin model	−1.0	−0.5	−1.2	−0.9	−0.7	−0.8	−1.5	−1.1	−0.6	−0.2
	BSJ model	−3.0	−1.8	−3.7	−2.8	−2.4	−2.2	−4.5	−3.4	−1.2	−0.5
$\overline{v}_3$	Standard	*1.319*	*1.206*	*1.362*	*1.267*	*1.228*	*1.333*	*1.494*	*1.326*	*1.308*	*1.166*
	No trpt. corr.	−0.1	−0.1	−0.2	−0.2	−0.2	−0.2	−0.1	−0.1	−0.2	−0.1
	Nelkin model	−0.9	−0.5	−1.2	−0.8	−0.7	−0.8	−1.5	−1.0	−0.6	−0.2
	BSJ model	−3.1	−1.5	−3.8	−2.6	−2.0	−2.0	−5.0	−3.4	−1.3	−0.3
SI_c	Standard	*1.507*	*1.322*	*1.638*	*1.490*	*1.428*	*1.657*	*1.797*	*1.537*	*1.617*	*1.337*
	No trpt. corr.	0.0	0.0	−0.1	−0.1	0.0	0.0	0.0	0.0	−0.1	0.0
	Nelkin model	−1.5	−0.9	−1.7	−1.3	−1.1	−1.1	−1.9	−1.6	−1.0	−0.4
	BSJ model	−5.6	−3.3	−6.5	−5.1	−4.4	−3.8	−7.6	−6.1	−2.5	−0.9
SI_b	Standard	*1.296*	*1.118*	*1.349*	*1.203*	*1.143*	*1.350*	*1.557*	*1.301*	*1.301*	*1.065*
	No trpt. corr.	−0.3	−0.2	−0.2	−0.4	−0.4	−0.4	−0.1	−0.3	−0.2	−0.1
	Nelkin model	−1.5	−0.8	−1.7	−1.2	−0.9	−1.0	−2.0	−1.6	−1.0	−0.3
	BSJ model	−5.6	−2.6	−6.5	−4.3	−3.2	−3.2	−8.4	−6.0	−2.7	−0.7

[a] $\delta_i(\zeta_i)$ = ratio of average flux (density) in region i (1 = fuel, 2 = canning, 3 = moderator) to that in the fuel; v_i = average neutron speed in region i; SI_i = spectrum index at position i (c = centre, b = boundary)

[b] Standard = transport correction, white boundary condition, KY scattering model

[c] Lattice characteristics are given in Appendix 1

Table 2. Influence of the transport correction and different scattering models on some characteristic quantities of the neutron distribution. Standard values in italics, the other numbers are the percentage deviations.

scription [24], from the experimentally observed scattering cross-section. The following expressions for $\bar{\mu}(E)$ were found

$$\bar{\mu}(E) = \begin{cases} \frac{4}{3}\sqrt{\frac{\sigma_0}{\sigma_s(E)}} - \frac{2}{3} & \text{(for H in } H_2O\text{)} \\ \sqrt{\frac{\sigma_0}{\sigma_s(E)}} - \frac{2}{3} & \text{(for D in } D_2O\text{)} \end{cases} \tag{16}$$

With the aid of K-7 THERMOS the importance of the transport correction was examined for a number of H_2O-, D_2O-, and H_2O/D_2O-moderated lattices. The lattice characteristics are given in Appendix 1. The integral quantities taken for this purpose are:

(i) The flux and density disadvantage factors (δ_i and ζ_i) for canning and moderator

$$\delta_i = \int_i \mathrm{d}\mathbf{r} \int_0^{E^*} \mathrm{d}E\, \Phi(\mathbf{r}, E) \Big/ \int_1 \mathrm{d}\mathbf{r} \int_0^{E^*} \mathrm{d}E\, \Phi(\mathbf{r}, E) \tag{17}$$

where the subscripts 1, 2, and 3 refer to fuel, canning, and moderator, respectively. A similar expression holds for ζ_i with $\Phi(\mathbf{r}, E)$ replaced by the neutron density $N(\mathbf{r}, E)$.

(ii) The average neutron speed in fuel and moderator, $\bar{v}_1$ and $\bar{v}_3$

$$\bar{v}_i = \int_i \mathrm{d}\mathbf{r} \int_0^{E^*} \mathrm{d}E\, vN(\mathbf{r}, E) \Big/ \int_i \mathrm{d}\mathbf{r} \int_0^{E^*} \mathrm{d}E\, N(\mathbf{r}, E) \tag{18}$$

(iii) The spectrum index in the fuel centre and in the moderator at the cell boundary (SI_c and SI_b)

$$SI_i = \frac{(Lu^{176} : Dy^{164}) \text{ activation ratio in the cell at } r_i}{(Lu^{176} : Dy^{164}) \text{ activation ratio in a thermal spectrum at } 20^\circ \text{ C}} \tag{19}$$

The standard values for these quantities are given in italics in Table 2. They have been obtained from K-7 THERMOS using the KY model, the transport correction, a thermal cut-off at 0.405 eV (for the sake of comparison with experiments), and twelve energy groups corresponding to the group division of the fast code SATAN. The deviation of these quantities from their standard values, resulting from the fact that the transport correction has not been applied, has been entered in the same table. These deviations are expressed in per cent, and owing to rounding-off errors their absolute accuracy is 0.1.

The transport correction decreases the scattering cross-section of the moderator and thereby its opacity. The neutrons will travel more easily through the moderator and their spatial distribution will be smoothed. This is entirely a transport effect, also noticeable in one-group calculations. It increases with the lattice pitch. In D_2O lattices,

where this correction is smaller, its influence on the spatial distribution will be less but still significant owing to the usual large pitches. This is in agreement with the δ_3 and ζ_3 changes in Table 2. The slight decrease of the canning disadvantage factors, when the transport correction is not applied, can probably be explained from the anisotropy of the neutrons that enter the cladding from the moderator. When no transport correction is applied, this effect will be more pronounced, and consequently the neutrons, owing to their forward peaking, pass more easily through the canning.

The transport correction reduces the 0th moment of energy transfer M_0, leaving the higher moments unchanged. It will therefore cause some spectrum hardening even in an infinite, homogeneous medium. This shows that the present transport correction is inconsistent for homogeneous-medium calculations, where the isotropic model should be strictly valid. Fortunately, this effect is small in pure moderators because of their small absorption cross-section. The transport correction can therefore be applied to treat approximately the much more important anisotropy effects in reactor cells. There is, furthermore, a secondary effect on the spectrum. Because of the reduced opacity, neutrons stay shorter in the moderator, which causes a slight hardening of the neutron spectrum. This is confirmed by Table 2, where a slight softening can be observed when the transport correction is not used.

Finally, it may be said that the transport correction has no significant influence on the spectrum, while it reduces the moderator disadvantage factors ζ and δ by up to 3.5 per cent in the most loosely packed H_2O lattice. According to Honeck [1], it accounts for more than 90 per cent of the first-order anisotropy. Thus, one may feel confident that the consequences of the assumption of isotropic scattering have been reduced to a discrepancy in the flux ratios which is well below 1 per cent. In power lattices, which are usually tightly packed and where the H_2O or D_2O is less dense owing to the higher temperatures—and sometimes the voids—this correction will be smaller and certainly adequate for design calculations.

(*b*) The WS cell concept reduces the true square or hexagonal cell to a circular one. This reduces the number of spatial variables to one only, and hence significantly facilitates the calculations. However, it is then no longer possible to treat exactly the two-dimensional unit cell, i.e., the perfect reflection conditions on the square or hexagonal boundary correctly simulating the infinitely extended surrounding medium cannot be applied. It seems natural, though, to use this reflective condition also at the circular boundary of the equivalent WS cell. It was Newmarch who pointed out that this leads to gross over-estimates of the moderator-to-fuel flux ratio in small cells [22]. This was confirmed by Thie [25]. A better boundary condition seems to be that of isotropic flux return (white boundary). It was first suggested by Honeck [23], who obtained good agreement with multigroup two-dimensional calculations for small cells [1]. Later, Weiss and the author [26] verified that even for the extremely tightly packed Thie-lattices the white boundary condition gave results that agreed well with the Monte Carlo values reported by Thie [25]. Recently, Carlvik reported good

agreement for a square H_2O cell between a one-dimensional transport calculation using the white boundary condition and a two-dimensional one with the true boundary condition [27]. The former gave a moderator-to-fuel flux ratio which was too low by only one per cent. Therefore, and also because the white and reflective boundary conditions give the same results for loosely packed lattices, it was decided to use the former throughout the calculations on all lattices. Thus, in design calculations, where one is interested in flux ratios rather than in the detailed flux distribution across a cell, use of the WS cell with a white boundary does not lead to unacceptable errors, even in tightly packed lattices.

(*c*) Three different scattering models for H and D bound in water have been incorporated in K-7 THERMOS. They are the BSJ, Nelkin, and KY model, and have been discussed earlier. With K-7 THERMOS the influence of the choice of model on the spatially-dependent quantities, δ and ζ, and on spectrum sensitive parameters, like $\bar{v}$ and SI, has been investigated. The results have been summarised in Table 2.

The choice of model will primarily influence the spectrum, and only through changes of the energy-averaged cross-sections the spatial distribution. This is illustrated by the negligible changes of δ and ζ when going from the physically most elaborate KY model to that of Nelkin. Use of the BSJ model gives still in some cases a significant over-estimation of δ_3 and ζ_3. Concerning the spectrum, it can be seen that, in agreement with the discussion in Section 2.2, the KY model produces the hardest and the BSJ model the softest spectrum. Again, the differences between the Nelkin and the KY model are smallest, especially in the heavy-water lattices 9 and 10. Also in loosely packed lattices the models differ less, because at the limit of well-thermalised media they all approximate the Maxwellian distribution owing to the detailed balance condition Eq. (4). At higher temperatures the models should approach the free-gas model—this is not true for the BSJ model—so that in power lattices at operating temperatures the differences between them will be smaller. It may be concluded that the KY model gives reliable results. Further improvements will influence the spectrum sensitive quantities probably by not more than 2 per cent, while they will be of no significance for the spatial distribution (δ and ζ).

*

To sum up it can be said that, from a physical viewpoint, the three basic approximations in K-7 THERMOS will be of little or no influence on its reliability for the lattices considered in this work. There is every reason to believe that this statement may be extended to include lattices of power reactors under operating conditions, on the understanding that they are not in the vicinity of control elements or other heterogeneities. In the fast codes that will be described later, additional approximations have been introduced for the sake of computational speed. Their effects will be discussed when their results are compared with those from K-7 THERMOS. However, before the fast methods are studied, the reliability of K-7 THERMOS will be tested against experiments as well. Only then may some value be attached to a possible agreement between its results and those from the fast codes.

3. COMPARISON OF K-7 THERMOS WITH EXPERIMENTS

3.1. General considerations

Although it was argued in the previous chapter that one may expect reliable results from K-7 THERMOS—using the KY model, the white boundary condition, and the transport correction—a confrontation of its results with "reality", i.e., with measurements, should provide the ultimate test of its reliability. A detailed test by comparing its neutron distribution $N(r, E)$ with the results from beam extraction measurements is not practicable in most of the lattices studied. One must therefore resort to a comparison of those integral properties of the neutron distribution which are also amenable to measurement. Such an integral quantity is the activity of foils or wires that have been irradiated in the reactor cell. If K-7 THERMOS correctly evaluates $N(r, E)$, then the integral properties of its density distribution should be correct too. The converse of this statement is not true, the agreement of activation profiles not necessarily implying the correctness of the detailed distribution. In the previous chapter it was found that changes from one energy-transfer model to another affected the spatial neutron distribution (δ and ζ) only slightly, while they caused significant changes in the spectrum. On the other hand, the transport correction hardly influenced the neutron spectrum, while it had a marked effect on the spatial distribution, especially in light-water lattices. Thus, a comparison with measurements should at least include the spatial density distribution obtained from the activation profile of an $1/v$ absorber as well as a spectrum-sensitive quantity like the spectrum index SI of Eq. (19). The following reasoning will show that such a comparison is sufficient to test the reliability of the calculated thermal-group constants.

From the viewpoint of design calculations there are two types of integral quantity necessary for an adequate representation of the thermal neutron properties in a lattice homogenisation. They are the flux ratios δ_i as defined by Eq. (17) and the spectral averaging factors (g-factors) for the cross-sections of all nuclides. In terms of these quantities the thermal utilisation factor f can be written as

$$\frac{1}{f} = \sum_{i=1}^{K} \frac{V_i}{V_1} \cdot \frac{\Sigma^0_{ai}}{\Sigma^0_{a1}} \cdot \frac{g_i}{g_1} \delta_i \qquad (1 = \text{fuel}) \tag{20}$$

where K is the number of different regions in the cell (in this work $K = 3$), V_i the volume of the ith region, Σ^0_{ai} the 2200 m/s absorption cross-section in region i, and g_i the spectrum averaging factor for the absorption cross-section in this region. g_i can be written as

$$g_i = \int_0^{E^*} \mathrm{d}E \, \Sigma_{ai}(E) \, \psi_i(E) \Big/ \Sigma^0_{ai} \, \overline{\Phi}_i \tag{21}$$

with

$$\psi_i(E) = \frac{1}{V_i} \int_i \mathrm{d}\mathbf{r} \, \Phi(\mathbf{r}, E) \tag{22}$$

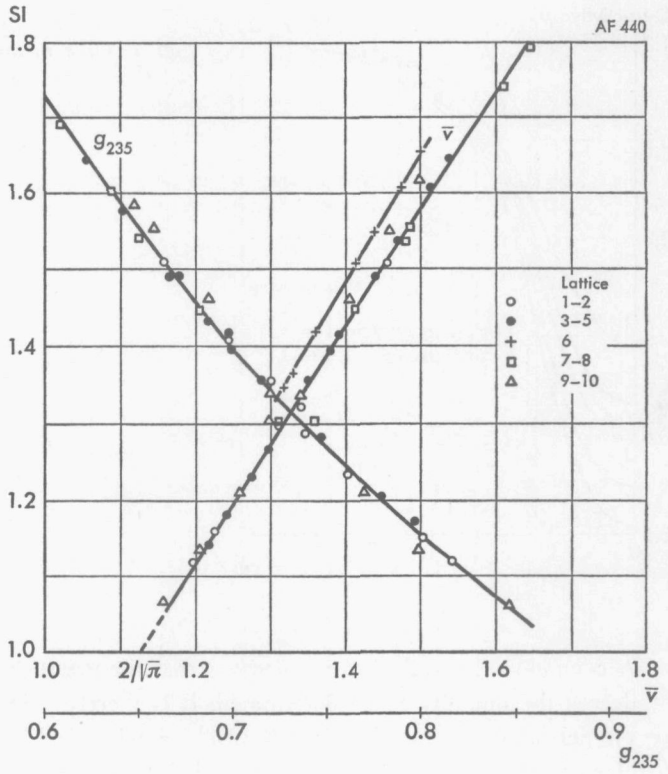

Fig. 2. Calculated SI-values versus g_{235} and the average speed $\bar{v}$ for the lattices 1 to 10.

$$\overline{\Phi}_i = \frac{1}{V_i}\int_i \mathrm{d}\mathbf{r} \int_0^{E^*} \mathrm{d}E\, \Phi(\mathbf{r}, E) = \int_0^{E^*} \mathrm{d}E\, \psi_i(E) \tag{23}$$

so that according to Eq. (17) the flux disadvantage factor can be written as the ratio of the two average fluxes

$$\delta_i = \overline{\Phi}_i / \overline{\Phi}_1 \tag{24}$$

Neither flux ratios nor g-factors can be measured directly. However, the flux ratio can be expressed in terms of the density ratio ζ_i and the average speeds $\bar{v}_i$ of Eq. (18):

$$\delta_i = \zeta_i\, \bar{v}_i / \bar{v}_1 \tag{25}$$

The ζ_i can be measured with $1/v$ absorbers, while the average speed and also the g-factor for U^{235} are strongly correlated with SI. This can be seen from Fig. 2, where SI has been plotted as a function of $\bar{v}$ and g_{235} for all lattices studied. Thus, one may expect that the calculated δ_i- and g_i-values will be correct when the measured and calculated ζ_i- and SI-values agree.

*

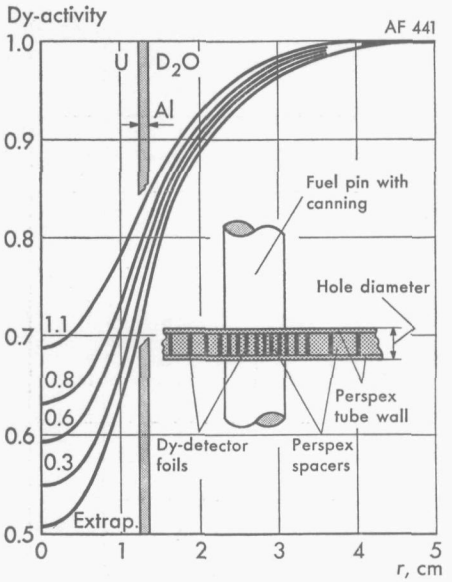

Fig. 3. Tube method used to illustrate the extrapolation principle in lattice 9: Change of activation profile for different hole (tube) diameters.

A common aspect of all experiments is that the measuring device disturbs to a certain degree the quantity to be determined. It is therefore important to evaluate carefully the perturbations introduced by the foils or wires and by their supports. This fact has often been underestimated or neglected. It has been the cause of the earlier discrepancies between measured and calculated density disadvantage factors for the BNL lattices [1], the Norwegian NORA lattices, and the Yugoslavian RB lattices [28, 29]. Only recently it was reported that Tunney had succeeded in resolving these discrepancies for the BNL lattices by carefully evaluating the perturbations [2]. For the NORA and RB lattices the same was done by the author and others [5].

To illustrate the magnitude of the effects involved, results of the tube method (to be described below) for the heavy-water lattices 9 and 10 are shown in Figs. 3 and 4 for different degrees of perturbation. It should be kept in mind that in these lattices with their rather thick fuel rods the effect of neutrons streaming into the fuel (one of the main perturbations) will be smaller than for thin rods. Furthermore, introduction of supports, tubes, etc., will disturb the distribution less in heavy water than in the optically much denser light water.

In Fig. 3 the diameter of the tube containing the Dy-Al detector foils was varied from 1.1 cm to 0.3 cm and then extrapolated to zero diameter. It should be observed that the perturbation seems to be approximately a linear function of the tube diameter. In Fig. 4 the extrapolation of the results of the tube method has been compared with that of a sector foil method, where the measuring device was geometrically (slab instead of cylinder) and physically (Al sheets were used instead of Plexiglas tubes) different. It is seen that the two entirely differently perturbed situations converged within 1 per cent of the same Dy activation profile for zero perturbation. This

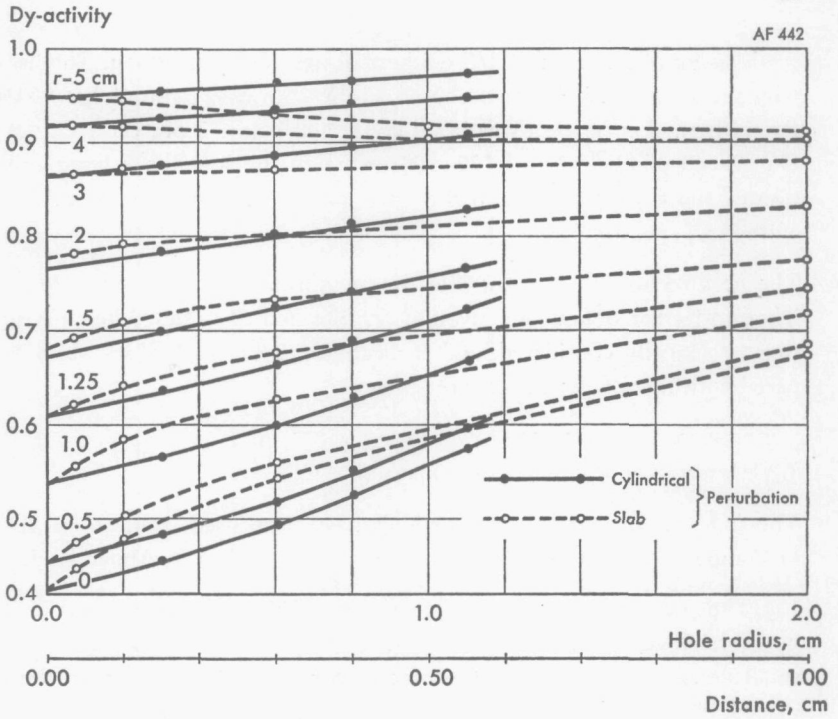

Fig. 4. Extrapolation of measured activity to zero hole radius or to zero distance between the fuel-rod halves (in lattice 10).

strongly suggests that the principle of the extrapolation used in the tube method is correct. At the same time, it should be remarked that measurements with sector foils, where the fuel element is radially cut, cause larger disturbances than measurements where small foils or wires are irradiated inside tubes. In the above-mentioned report [5] more examples are given of the effect of the perturbation on the activation profile. It is shown there that for a tubular fuel element even the shape of the activation profile can change.

Another correction that has been applied to the activation measurements is the subtraction of the activity caused by epithermal neutrons. This is often done by means of a cadmium-ratio measurement. However, Cd-ratio measurements should be avoided for two reasons. Firstly, the experimental definition of the thermalisation range by an effective cadmium cut-off is somewhat vague, since it depends on the spectrum of the neutron distribution, its isotropicity and on the variation of the detector cross-section with energy. Secondly, especially in tightly packed lattices with hard spectra, the introduction of cadmium causes large disturbances and, hence, leaves undesirable uncertainties in the experimental results. Cd-ratio measurements can be avoided by using detector materials that have a low epithermal cross-section (resonance integral) compared with their thermal cross-section, like Dy^{164} and Lu^{176}. In this case the epithermal correction will be small and can be theoretically determined under the

crude assumption of a flat $1/E$ epithermal neutron distribution. This is also the reason why the spectrum index was chosen as the activation ratio of $Lu^{176} : Dy^{164}$, Eq. (19). Its epithermal correction was in all cases well below 2 per cent. Earlier attempts with Cu instead of Dy^{164} failed [28, 30] owing to the sometimes large epithermal correction of the Cu-activation and the uncertainties in both its resonance integral and the epithermal spectrum.

The next section briefly describes the measuring techniques that are used at different laboratories for obtaining activation profiles and SI-values. Their perturbation evaluation is critically considered, and in Section 3.3 the K-7 THERMOS results are compared with those from the experiments.

3.2. *Description of experimental methods*

The following four activation methods have been used in the H_2O-, D_2O-, and H_2O/D_2O-moderated single-pin lattices, which are described in Appendix 1.

(*a*) The *pin method,* which is due to Tas [31], has been applied in lattices 4 and 6 by Bryhn-Ingebrigtsen [5], and in lattice 7 by Tas. The method consists of irradiating small detector pins in specific positions in fuel and moderator. In the fuel they were placed in holes drilled axially into the pellets, while in the moderator they were positioned in Plexiglas holders. This introduces three types of disturbance: the perturbation caused by the pin holder, the perturbation effect due to each individual pin, and the pin interaction. Concerning the first effect, no correction was made, since it was believed that Plexiglas closely simulates the water. However, recent investigations of Tunney [32] have shown that its effect is not entirely negligible and the amount of Plexiglas should be minimised or, preferably, extrapolated to zero.

In lattices 4 and 6 Cu-pins were irradiated in 5.5-mm-deep holes in the fuel, while the Plexiglas holder in the moderator was 1 mm thick. They were protected against fission products by a layer of lacquer. After irradiation they were β-counted and a Cd-ratio measurement provided the epithermal correction. The pin perturbations were determined by varying the number of pins and their diameters, which ranged from 0.6 to 1.5 mm. It was assumed that the two perturbations are a linear function of the number of pins and of the pin volume. Although the interaction effect will be different in moderator and fuel, which makes uniform extrapolation difficult, this is no serious drawback because the effect is very small [33]. However, it can be shown that the extrapolation to zero pin diameter should, at least in the moderator, be a linear function of the pin radius and not of its volume. This will cause the extrapolated activity in the moderator to be still too low. In the fuel this effect will be less serious, since pins and fuel have approximately the same absorption cross-section.

In lattice 7 Dy-Al pins (5 % Dy in Al) of 0.5 mm diameter were used. The holes in the fuel were only 2.5 mm deep and the Plexiglas pin holder was also thinner than in the two other lattices, namely, 0.2 mm. The pins did not have to be protected

against fission products, since only the 47 keV gammas were counted. The epithermal correction, which is very small for Dy, was obtained theoretically. No correction for the pin interaction was applied, while the flux depression caused by each individual pin was computed by MICROFLUX [8] and found to be 3.0 per cent in the moderator and 0.5 per cent in the fuel.

(*b*) The *rolled wire method* is due to Wikdahl and Åkerhielm [34] and has been used by Bryhn-Ingebrigtsen to obtain density disadvantage factors in the lattices 1, 3, 4 and 5 [28, 5]. Cu-wires laid along the principal traverse axes of the reactor cell in holes drilled radially through three fuel elements were irradiated. They were protected against fission products by lining the holes with tubes made of Al-foil. After irradiation they were rolled to Cu-tapes, which were then β-counted by an automatic scanner. The epithermal correction was obtained from a Cd-ratio measurement.

In all lattices, except No. 1, the results were corrected for the inflow of neutrons through the aluminium and for the perturbation of the wire itself. This was done by irradiating wires of various thicknesses in holes with different diameters. The two effects were assumed to be independent of each other and to be a linear function of the wire cross-section and the area of the gap between wire and fuel. However, the flux depression caused by the wire should have been taken as linearly dependent on its radius, while the extrapolation to zero gap area shown in Fig. 7 a also suggests a higher order dependence.

(*c*) The *tube method* in its present version is due to Takač and Krčevinac [35] and has been applied by them to the lattices 4, 9 and 10. Small Dy-Al detector foils were placed in Plexiglas tubes, separated by cylindrical spacer pellets also made of Plexiglas. These tubes were then inserted in radial holes drilled in a fuel element at an angle of 27.5° to the rod-to-rod direction. This direction is representative of the circular cell, and the measured activation profiles, after the usual corrections, can therefore be directly compared with the computed ones [36]. The perturbation due to the Plexiglas—and the relatively small amount of detector material—was uniformly extrapolated to zero. To that end, a series of measurements was carried out with foils of different sizes and Dy contents. These foils were irradiated in tubes with different inner and outer diameters. In all these measurements the physical composition of the measuring device was kept the same. For each tube diameter the individual points were fitted to a Bessel function in the fuel and a polynomial in the moderator [5]. At suitably chosen radial distances the activation was read from the activation profile curves for the different tube diameters found in this way. These activations were then extrapolated to zero tube size using a second-order polynomial of the diameter. As follows from Fig. 4, this extrapolation is linear in the moderator ($r > 1.25$ cm), while it deviates slightly from the linear shape inside the fuel rod. It can also be concluded from Fig. 4 that the extrapolation technique used here produces reliable results, since it agrees well with the results of the same kind of extrapolation for a differently perturbed situation. The epithermal correction, which is very small for Dy, has been obtained by Cd-ratio measurements.

(*d*) The *sector foil method* has been used in two variants. In lattices 7 and 8 it was applied by Tas to determine density disadvantage factors. In the lattices 1–5, 7 and 8 it was used by Smit to measure the variation of the spectrum index SI across a cell [30, 37].

In the first variant, Dy-Al foils, containing 5 wt. % dysprosium, with thicknesses 0.1 mm, 0.05 mm, and 0.025 mm were used. Two foils of equal thickness were activated, one in the fuel and the other in the moderator. The foil areas were equal to the fuel part and the moderator part of the unit cell. The foil in the fuel was not protected against fission products, because the activations were determined by measuring the 47 keV gammas. In the moderator use of a support was also avoided, because the foils were pressed against the canning. The density disadvantage factor ζ_3 is then the ratio of the activities of the two foils, after correcting for the epithermal activation, the foil sizes and the non-$1/v$ absorption of the detector. The only perturbation in this method arises from the foils themselves. It has been evaluated from multigroup calculations in slab geometry with MICROFLUX [8]. It was also determined by extrapolating the results obtained with the three different foil thicknesses to zero. In the moderator this extrapolation should be proportional to $d \ln (1/d)$, where d is the foil thickness. The epithermal correction was found theoretically.

The second variant has been developed by Smit [30, 37] to measure the spectrum-sensitive index SI, defined from Eq. (19). It is consequently the only experimental technique described here which provides information on the adequacy of the energy-transfer models used in the calculations. In lattices 1–5 the spatial variation of SI inside a unit cell was measured, while in the lattices 7 and 8 only its average values in fuel and moderator were obtained.

In the first five lattices 0.125-mm-thick Dy-Al and Lu-Al foils (5.2 % Dy and 3.9 % Lu) were irradiated in the lattice as well as in the moderator. In the fuel thin catcher foils of copper protected them against fission products, thus minimising streaming effects, because copper has roughly the same absorption cross-section as the fuel. Plexiglas supports were used in the moderator. The foils were then β-counted, being laid under different Cu-covers in which holes or slits had been punched at varying radial positions. Thus, the spatial dependence of the foil activity could be measured at well-defined distances from the centre of the cell, since only the β-activity of the uncovered parts was registered. The perturbations will have a different effect on the SI-values than on the usual activation profiles, because many errors cancel out in the double-ratio SI.

Normally, the Plexiglas support has not been corrected for, although a preliminary attempt in lattice 4 showed that its presence increases the SI-values in the moderator by (0.8 ± 0.3) per cent. No corrections were made for the perturbations caused by the foils themselves, and consequently resulting experimental data should be treated with some reserve.

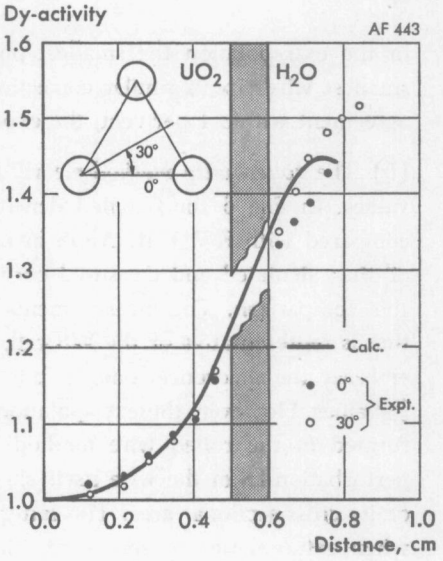

Fig. 5. Comparison of calculated and experimental (pin method) Dy-activation profiles in Lattice 7.

In lattices 7 and 8 only averages of SI in fuel and moderator were measured. The foils were 0.1 mm thick and contained 10 wt. % Lu or Dy in Al. The Dy-foils were not protected against fission products, since 47 keV gammas were counted there. The low counting rate of the Lu-foils, however, required protection, the fission product activity otherwise becoming relatively too strong. Like in the first variant, no supports were used in the moderator. Corrections for the different flux depressions caused by the Lu- and Dy-foils were calculated using MICROFLUX [8]; no extrapolation was tried. The epithermal correction, which is small owing to the choice of the detector materials, was also found theoretically.

3.3. Comparison of theory with experiment

The comparison of K-7 THERMOS with measurements is summarised in Table 3 and Figs. 5–9. The results will be discussed below per experimental method.

(*a*) The *pin method* agrees best with the theoretical values in lattice 7, where most care was taken to eliminate and evaluate the perturbations. Fig. 5 shows for this lattice the comparison with the detailed Dy-activation profiles measured in two directions. The theoretical curve has been corrected to include the epithermal contribution, which varied from 7.4 per cent in the fuel to 5.5 per cent in the moderator. In lattices 4 and 6 the experimental ζ_3-values lie lower than the theoretical ones by 1.7 and 2.4 per cent, respectively, which is more than the quoted experimental uncertainty. However, in these lattices the extrapolation of the pin perturbation to zero pin size was taken to be linear with its volume rather than with its radius. This leads to a too low value for ζ_3, as can be seen in Fig. 7 b, where the two types of extrapolation are shown to give ζ_3-values that differ by 2.6 per cent for the rolled wire method. Since

in the extrapolation the smallest pin size (0.6 mm diameter) was the same as the smallest wire size, a similar correction may be expected here, which would bring the agreement within 1 per cent, the experimental values being the highest.

(*b*) The *rolled wire method* clearly gives poorer agreement with the K-7 THERMOS values. In Fig. 6 the detailed density distributions, measured in two directions, are compared with K-7 THERMOS in lattice 4. Apart from the slightly different shapes of the calculated and measured curves in the fuel, not much can be concluded from this comparison. The measurements should rather have been made in the direction that is representative of the WS cell, namely, 27.5°. Although the experimental curves embrace the theoretical one, it follows from Table 3 that they still lead to different ζ_3-values. However, the extrapolation of the perturbations has not been properly performed in the rolled wire method. This is illustrated for lattice 4 in Fig. 7. The perturbation from the wire itself should be a linear function of its radius rather than of its cross-sectional area. The latter dependence was assumed by Bryhn-Ingebrigtsen when extrapolating to zero wire thickness and is represented by the full line in Fig. 7 b. The dashed line is based on the former dependence, which is physically more correct. The extrapolated ζ_3-values are seen to differ by as much as 2.6 per cent. Fig. 7 a suggests furthermore that the perturbation from the gap between the wire and the hole in the fuel is not linearly dependent on its surface either. Another correction of 1 per cent is hidden here. Hence, in lattice 4 the final result for ζ_3 should be in-

Method	Lattice				
	1	2	3	4	5
K-7 THERMOS					
ζ_2	1.130	1.131	1.183	1.182	1.182
ζ_3	1.374	1.502	1.466	1.577	1.661
SI_c	1.507	1.322	1.638	1.490	1.428
SI_b	1.296	1.118	1.349	1.203	1.143
Pin method					
ζ_2	—	—	—	—	—
ζ_3	—	—	—	1.55 ± .02	—
Rolled wire					
ζ_2	—	—	1.16 ± .01	1.17 ± .01	1.17 ± .01
ζ_3	1.28	—	1.40 ± .01	1.53 ± .01	1.57 ± .01
Tube method					
ζ_2	—	—	—	1.19	—
ζ_3	—	—	—	1.57	—
Sector foil					
ζ_2	—	—	—	—	—
ζ_3	—	—	—	—	—
SI_c	1.51 ± .03	1.38 ± .03	1.68 ± .04	1.50 ± .03	1.43 ± .03
SI_b	1.34 ± .03	1.19 ± .03	1.47 ± .04	1.25 ± .03	1.18 ± .03

Table 3. Comparison of K-7 THERMOS with measurements.

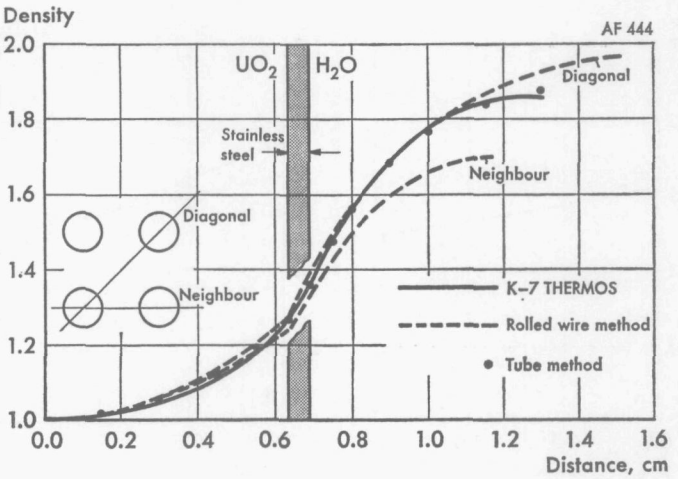

Fig. 6. Comparison of calculated and measured neutron density distributions in lattice 4.

creased by 3.6 per cent owing to an insufficient extrapolation. The crude assumption will be made that the same 3.6 per cent correction should be applied to the experimental ζ_3-values in the lattices 3 and 5 too. In lattice 1 no corrections were made at all for the perturbations caused by the 1.0-mm-thick Cu-wire and the 1.2 mm hole

Lattice					Method
6	7[a]	8[a]	9	10	
					K-7 THERMOS
1.171	1.183	1.193	1.266	1.286	ζ_2
1.536	1.293	1.379	1.603	1.849	ζ_3
1.657	1.734	1.486	1.617	1.337	SI_c
1.350	1.570	1.317	1.301	1.065	SI_b
					Pin method
1.17 ± .01	—	—	—	—	ζ_2
1.50 ± .02	1.292 ± .005	—	—	—	ζ_3
					Rolled wire
—	—	—	—	—	ζ_2
—	—	—	—	—	ζ_3
					Tube method
—	—	—	—	—	ζ_2
—	—	—	1.59	1.85	ζ_3
					Sector foil
—	—	—	—	—	ζ_2
—	1.29 ± .01	1.47 ± .02	—	—	ζ_3
—	1.72 ± .04	1.57 ± .02	—	—	SI_c
—	1.59 ± .04	1.32 ± .02	—	—	SI_b

[a] Dy-activation "disadvantage factors" and SI averages in fuel and moderator are given here.

Table 3 (continued)

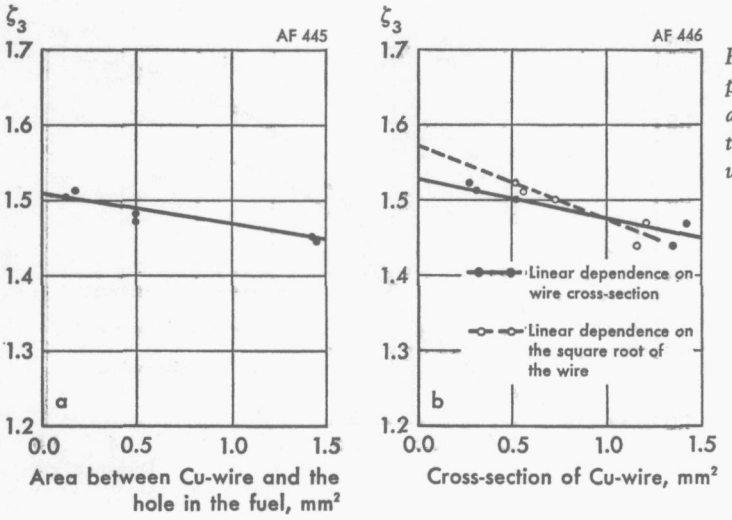

Fig. 7. Lattice 4: Extrapolation of ζ_3 to zero gap area (a) and zero Cu-wire thickness (b) using rolled-wire results.

through the fuel. A crude estimate of the necessary correction can be made by using Fig. 7. One finds then that the experimental ζ_3 has to be raised by 6.9 per cent.

After these extra corrections, the discrepancies between calculated and measured ζ_3-values have been reduced to 0.2, 1.0, -0.6, and 2.0 per cent for the lattices 1, 3, 4, and 5, respectively. This agreement is satisfactory, except for lattice 5.

(*c*) The *tube method* gives in all cases good agreement with the theoretical curves and ζ_3-values. This follows from Figs. 6 and 8, as well as from Table 3. In this method the extrapolation to zero perturbation has been done in a consistant manner and the remaining error will be less than 1 per cent. The difference between theoretical and experimental ζ_3-values is 0.7, 0.8, and -0.5 per cent in the lattices 4, 9, and 10, respectively.

(*d*) The *sector foil method* results for lattices 7 and 8 have been carefully corrected for the perturbations. In lattice 7 its results, both for ζ_3 and the spectrum index, agree well with the K-7 THERMOS calculations. The differences are within the quoted experimental error as follows from Table 3. However, in lattice 8 there is a striking discrepancy caused by the breaking down of the validity of the WS cell concept in this strongly heterogeneous, open hexagonal lattice. Thus, neither K-7 THERMOS nor any other one-dimensional thermalisation code can be used on such types of lattice.

The SI measurements in the lattices 1–5 show some disagreement with the calculations as can be seen from Fig. 9 and Table 3. The disagreement in lattice 2 must probably be ascribed to a bad experiment. The disagreement in the moderator which increases with the hardness of the spectrum may very well be explained by the lack of a perturbation evaluation, because in lattice 7, where the spectrum is hardest but where the perturbations have been kept small and evaluated theoretically, there is no such discrepancy. Even the perturbation from the foil holder in lattices 1–5, which in

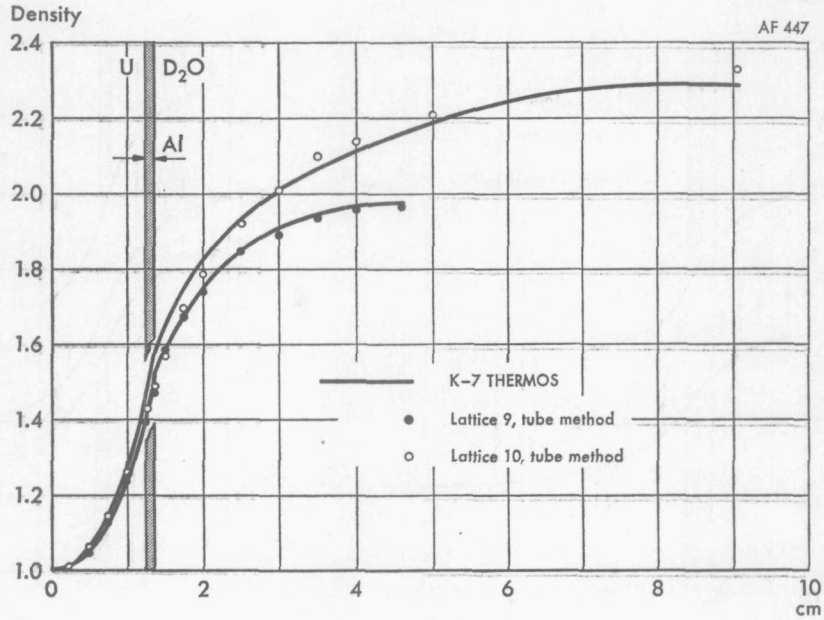

Fig. 8. Comparison of K-7 THERMOS with measured neutron density distributions in lattices 9 and 10.

lattice 4 was found to be (0.8 ± 0.3) per cent, has not been taken into account in Table 3.

In conclusion it can be stated that the experimental results have given additional confidence in the K-7 THERMOS calculations. Those measurements where the perturbations were carefully evaluated showed good to excellent agreement with the calculations. In the Norwegian NORA lattices 1, 4, and 5 the sector foil method for the spectrum index produced good agreement in the fuel, although the values in the moderator are too high which is probably caused by the neglecting of the perturbing effects of the foils and their supports. In lattice 4, the tube method reproduced the theoretical ζ_3-values very well. In the Dutch PUK lattice 7, the perturbations were kept small and carefully evaluated. All measurements performed in this lattice gave good agreement with the K-7 THERMOS results. In the Yugoslavian RB lattices 9 and 10, good agreement was also reached between the tube method results and those from the calculations. Whenever disagreement was noticed, it could be explained by an inaccurate or even lacking perturbation correction. It has been shown, for example, that a physically more plausible extrapolation of the perturbations in the rolled wire method would bring its results to within 2 per cent of the calculated ζ-values for the NORA lattices 1, 3, 4 and 5. The only exception is the open hexagonal lattice 8, where the open fuel positions have disturbed the regularity of the lattice to such a degree that the WS cell concept has become invalid. Such lattices, however, seldom or never occur in true power reactors. It is thus obvious that the agreement of K-7 THERMOS with experiments holds for regular lattices only. The many heterogeneities

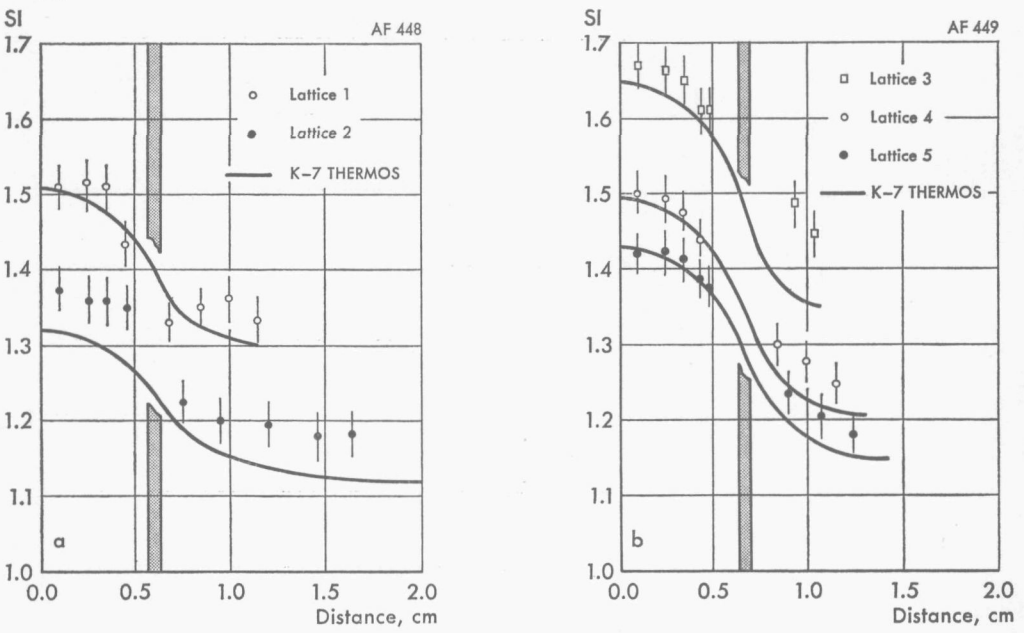

Fig. 9. Comparison of theoretical and experimental SI-values.

in a power reactor, such as control elements and water gaps, will require both a theoretical and an experimental investigation of the changes in neutron distribution and spectrum near these heterogeneities. This falls, however, outside the scope of the present work, which has been restricted to regular lattices.

4. FAST METHODS FOR EVALUATING THERMAL-GROUP CONSTANTS IN THREE-REGION CELLS

4.1. General considerations

In fuel-cycle studies of power reactors some types of calculation may have to be repeated thousands of times. It is therefore imperative for reactor design methods that they share speed and accuracy. Unfortunately, these two requirements seem to be practically incompatible. Even on a GE-625 or a CDC-3600 computer the code K-7 THERMOS needs from 2 to 3 minutes for a pin-cell calculation. It contains three time-consuming parts, namely, the evaluation of the scattering matrix and of the transport kernel, and the iteration process. Of these, the scattering matrix could, in principle, be calculated once and for all for a fixed group structure and at a given number of temperatures between which linear interpolation can be used. These matrices could then be stored on the magnetic library tape, together with the other basic cross-section data. In this way the computation time needed for the KY kernel could be eliminated, which would mean a reduction of the total running time of

about 50 per cent. By choosing Carlvik's method to evaluate the transport kernel [21] one might cut down the calculation time for this kernel by 50 per cent. However, in the iteration process no savings are possible as long as the multishell, multigroup approach is maintained. One of the main drawbacks there is that the coefficients of the iteration matrix have to be computed again for each iteration step. Thus, if K-7 THERMOS is carefully rewritten and reorganised, its running time per case might be reduced to 0.5–1.0 minute. However, this is still prohibitively long for use in design studies, especially for BWR lattices.

It seems unavoidable that extra simplifications must be introduced to reduce the calculation times. Fortunately, no detailed neutron distributions are needed and, as was pointed out in Section 3.1, knowledge of the flux ratios and the spectrum-averaging g-factors [cf. Eqs. (24) and (21)] is sufficient for design purposes. Incidentally, it should be noted that K-7 THERMOS cannot produce the two-dimensional neutron distribution either, owing to the WS cell approximation.

From now on the calculational methods will be restricted to three-region lattices of the type: fuel rod, canning, moderator. For this type of lattice a very fast *and* accurate one-group calculation of the flux ratios has been developed by Weiss [11]. This method, which has been named AMCLA, is a consequent extension of the almost classic ideas of Amouyal, Benoist, and Horowitz (ABH) [38] to include also the cladding. AMCLA will be briefly described in the next section, because it is an essential unit of the fast codes DATAPREP-II [11] and SATAN [39] to which the last two sections of this chapter are devoted.

4.2. Flux-ratio calculations in one group: the AMCLA code

The principles and assumptions on which AMCLA is based are:

(*a*) "White interface" between moderator and canning, i.e., the neutrons that pass this interface will "forget" their original direction of motion and continue their flight as if coming from an isotropic flux. This is the isotropic incident flux (IIF) approximation, which is also basic to the ABH method [38]. It allows for the separate treatment of the canning-plus-fuel region and the moderator.

(*b*) Canning and fuel will be treated by a collision probability technique. Here the approximation will be made that, for calculating the collision probabilities from one region to another, the collision density after the first collision may be taken as flat. This flat-flux approximation (FFA) has been used with great success by Fukai [40] for tightly packed slab lattices. This assumption is a deviation from the original ABH method, where the first and second collisions were treated exactly. In AMCLA, however, six collision probabilities must be evaluated and in the FFA there exist three relations between them which means a considerable saving of machine time.

(*c*) Following the original ABH work, diffusion theory will be used in the moderator, with the effective boundary condition

$$\frac{\mathrm{d}}{\mathrm{d}r}[\ln \varphi(r)] = \frac{\Sigma_{t3}}{\lambda_\infty(R_2\Sigma_{t3})} \qquad (\text{at } r = R_2) \tag{26}$$

where Σ_{t3} is the total cross-section in the moderator, R_2 the radius of the canning, and λ_∞ the effective linear extrapolation length for a black cylinder embedded in an infinite non-absorbing medium, which can be approximated [5] by

$$\lambda_\infty(x) = \left\{ \begin{array}{ll} \dfrac{0.2442}{0.4316 + x} + 0.7675 & (0 \le x \le 1) \\ \dfrac{0.292}{0.28 + x} + 0.7104 & (x > 1) \end{array} \right\} \tag{27}$$

One might suspect that this approximation gives bad results in tightly packed lattices where the diffusion theory should break down. However, it has been shown by Weiss [41] that owing to a cancelling of the two errors—the IIF approximation, and use of diffusion theory with λ_∞ instead of the true λ which should also account for the finiteness of the moderator—this method gives good results for the whole range of lattice sizes.

(*d*) The source will be assumed flat, isotropic and only present in the moderator.

With these assumptions as a starting point, the following expressions for the flux disadvantage factors of canning and moderator can be derived in a straightforward manner. The derivation is given in the Kjeller Report [11] and will not be repeated here.

$$\delta_2 = \Sigma_{a1} V_1 \Gamma_2 / \Sigma_{a2} V_2 \Gamma_1 \tag{28}$$

$$\delta_3 = 2 R_2 \Sigma_{a1} \left(\frac{R_1}{R_2}\right)^2 \left\{ \frac{1 - \Gamma_1 - \Gamma_2}{\Gamma_1} + \left(1 + \frac{\Gamma_2}{\Gamma_1}\right)\left[\frac{3x}{8} \cdot \frac{F(R_3/R_2)}{1 - (R_2/R_3)^2} + \frac{3}{4}\lambda_\infty(x)\right]\right\} \tag{29}$$

where

$$F(z) = \frac{(\ln z^2)}{1 - 1/z^2} + \frac{1}{2z^2} - \frac{3}{2} \tag{30}$$

and Γ_1 (Γ_2) is the fuel (canning) blackness, i.e., the probability that a neutron entering the canning from the moderator will be absorbed in the fuel (canning). In case of zero absorption in the canning, $\Gamma_2 = 0$, and Eq. (29) reduces to the familiar ABH formula. The influence of the canning on the moderator-to-fuel flux ratio δ_3 comes from the Γ_2/Γ_1 containing terms inside the brackets of Eq. (29). It has been found to lie well below 1 per cent for the lattices considered in this work.

The problem has henceforth been reduced to the evaluation of the probabilities Γ_1 and Γ_2. In the Kjeller Report [11] it has been shown that they can be expressed in terms of first collision probabilities:

$$\Gamma_1 = (1 - c_1)\,\frac{P_1(1 - c_2 P_{22}) + c_2 P_2 P_{21}}{(1 - c_1 P_{11})(1 - c_2 P_{22}) - c_1 c_2 P_{12} P_{21}} \tag{31}$$

$$\Gamma_2 = (1 - c_2)\,\frac{P_2(1 - c_1 P_{11}) + c_1 P_1 P_{12}}{(1 - c_1 P_{11})(1 - c_2 P_{22}) - c_1 c_2 P_{12} P_{21}} \tag{32}$$

where c_i is the number of secondaries per collision in region i, i.e., $c_i = \Sigma_{si}/\Sigma_{ti}$. P_1 and P_2 are the first collision probabilities in fuel and canning owing to an isotropic incident flux on the canning. The remaining four probabilities P_{ij} are defined as the probability that a neutron born uniformly and isotropically in region i will suffer its next collision in region j.

Owing to the FFA, three of these first collision probabilities can be expressed in terms of the other three:

$$P_{12} = 1 - [P_{11} + (S/4\,V_1\,\Sigma_{t1})\,P_1] \tag{33}$$

$$P_{21} = V_1 \Sigma_{t1} P_{12}/V_2 \Sigma_{t2} \tag{34}$$

$$P_{22} = 1 - [P_{21} + (S/4\,V_2 \Sigma_{t2})\,P_2] \tag{35}$$

where S is the surface of the canning, i.e., $2\,\pi R_2$.

Only the probabilities P_1, P_2 and P_{11} need therefore be calculated. The former two can be represented by the following two single integrals:

$$P_1 = \frac{4}{\pi}\int_0^{\varphi_0} \mathrm{d}\varphi \cos\varphi\,[Ki_3(l_1 \Sigma_{t2}) - Ki_3(l_1 \Sigma_{t2} + l_2 \Sigma_{t1})] \tag{36}$$

$$P_2 = 1 - P_1 - \frac{4}{\pi}\left[\int_0^{\varphi_0} \mathrm{d}\varphi \cos\varphi\, Ki_3(2 l_1 \Sigma_{t2} + l_2 \Sigma_{t1}) + \int_{\varphi_0}^{\pi/2} \mathrm{d}\varphi \cos\varphi\, Ki_3(l_3 \Sigma_{t2})\right] \tag{37}$$

where

$$l_1 = R_2 \cos\varphi - \sqrt{R_1^2 - R_2^2 \sin^2\varphi}$$

$$l_2 = 2\sqrt{R_1^2 - R_2^2 \sin^2\varphi}$$

$$l_3 = 2\,R_2 \cos\varphi$$

$$\varphi_0 = \arcsin\,(R_1/R_2)$$

The P_{ij} probabilities are double integrals, but fortunately, P_{11}, the non-escape probability from an infinitely long, black cylinder, can be expressed in Bessel functions of the second kind [42]:

$$P_{11} = 1 - \frac{2}{3}\Big\{2\Big[xK_1(x)\,I_1(x) + xK_0(x)\,I_0(x) - 1\Big] + K_1(x)\,I_1(x)/x - K_0(x)\,I_1(x) + K_1(x)\,I_0(x)\Big\} \tag{38}$$

which, for small and large arguments, can be approximated by

$$P_{11} = \frac{4}{3}x + \frac{1}{2}x^2 \ln\left(\frac{x}{2}\right) + \frac{1}{2}x^2\left(\frac{5}{4} - \gamma\right) \qquad (x \leq 0.1) \tag{38 a}$$

$$P_{11} = 1 - 1/2x + 3/32x^3 \qquad (x \geq 6) \tag{38 b}$$

with Euler's constant $\gamma = 0.5772157\ldots$ and $x = R_1\, \Sigma_{t1}$.

The calculation of the Bessel functions and of the Bickley function Ki_3 is done from their Chebyshev expansion coefficients as described in Appendix 2. The integration over φ in Eqs. (36) and (37) is performed using Simpson's rule with repeated halving of the intervals until an accuracy of better than 0.5 per cent is reached. From the result thus converged, 0.35 times the last difference is subtracted, a rest correction which has been found empirically.

AMCLA has been tested on numerous occasions against exact one-group transport calculations. Errors of more than 1 per cent were observed only very rarely. An example of such a comparison for eight of the lattices investigated here is given by the author and Tas [39]. One may safely conclude that AMCLA produces almost exact one-group flux ratios in cylindricalised single-pin cells. Its calculation time on the GE-625 computer is extremely short, namely, between 0.015 and 0.035 seconds. Because of this rather unique combination of accuracy and speed, it will be an indispensable calculational unit in the two fast methods to be described in the following sections.

4.3. One-group approach with effective cross-sections: the code DATAPREP-II

As was mentioned earlier in this chapter, a straightforward numerical treatment of the integral transport equation (1) in the multishell, multigroup approach Eq. (10) would be too lengthy for design calculations. However, Eq. (1) can be simplified to a one-group transport problem for the spatial flux $\varphi(\mathbf{r})$ by integration of it over the energy.

$$\overline{\Sigma}_t(\mathbf{r})\, \varphi(\mathbf{r}) = \int d\mathbf{r}'\, \overline{T}(\mathbf{r}' \to \mathbf{r}) \left[\overline{\Sigma}_s(\mathbf{r}')\, \varphi(\mathbf{r}') + \overline{S}(\mathbf{r}') \right] \tag{39}$$

where use has been made of the property Eq. (3) that the scattering kernel integrates to $\Sigma_s(\mathbf{r}, E)$, and with

$$\varphi(\mathbf{r}) = \int_0^{E^*} dE\, \Phi(\mathbf{r}, E) \tag{40}$$

$$\overline{S}(\mathbf{r}) = \int_0^{E^*} dE\, S(\mathbf{r}, E) \tag{41}$$

Table 4. Flux disadvantage factors from three different methods (BSJ scattering model, 0.632 eV cut-off).

Lattice	K-7 THERMOS		Percentage deviation from K-7 THERMOS			
			One-group calculation		DATAPREP-II	
	δ_2	δ_3	δ_2	δ_3	δ_2	δ_3
1	1.098	1.276	−0.2	−0.9	+0.6	+1.0
2	1.102	1.379	−0.2	−1.2	+1.1	+1.8
3	1.139	1.341	−0.4	−1.2	+0.7	+0.5
4	1.140	1.426	−0.5	−1.4	+1.7	+1.6
5	1.141	1.492	−0.5	−1.5	+2.2	+3.3
7	1.131	1.204	−0.4	−0.7	+0.1	+1.4
8	1.141	1.269	−0.3	−0.9	+0.8	+1.5
9	1.203	1.470	−1.2	−1.0	−0.1	+2.7
10	1.222	1.689	−1.2	−1.3	+0.7	+3.6

$$\overline{\Sigma}_{s,t}(\mathbf{r}) = \int_0^{E^*} \mathrm{d}E\, \Sigma_{s,t}(\mathbf{r}, E)\, \Phi(\mathbf{r}, E)/\varphi(\mathbf{r}) \tag{42}$$

$$\overline{T}(\mathbf{r} \to \mathbf{r}') = \int_0^{E^*} \mathrm{d}E\, T(\mathbf{r} \to \mathbf{r}', E) \int_0^{E^*} \mathrm{d}E'\, \Sigma_s(\mathbf{r}, E' \to E)\, \Phi(\mathbf{r}, E') \Big/ \overline{\Sigma}_s(\mathbf{r})\, \varphi(\mathbf{r}) \tag{43}$$

Actually, two transport kernels $\overline{T}$ should have been defined, one acting on $\overline{\Sigma}_s\varphi$, Eq. (43), and the other on the source $\overline{S}$. However, in order to take advantage of the simplification to the one-group model, the two-dimensional transport kernel $\overline{T}$ will not be evaluated from Eq. (43), which would still need an equally time-consuming calculation as before owing to the energy integration. If one notices that the energy dependence of the transport kernel is only through $\Sigma_t(\mathbf{r}, E)$, it seems natural to approximate $\overline{T}$ by computing it in the one-group picture using $\overline{\Sigma}_t(\mathbf{r})$. The error thus incurred was investigated by comparing of flux ratios from multigroup K-7 THERMOS or MICROFLUX calculations with their values obtained from one-group transport calculations. The effective cross-sections used in the latter were the spectrum averages from K-7 THERMOS or MICROFLUX. This comparison was done using the BSJ model and a 0.632 eV cut-off. Its results are given in Table 4. The error is seen to be small and it is largest in lattices where Σ_t varies most strongly with energy. It can be shown that this approximation reduces the transport between nearby points, while it increases the transport kernel elements connecting points that lie farther apart. In this respect its effect is similar to that of the transport correction; the neutron distribution becomes flatter, which explains the negative sign of the errors in Table 4.

This procedure of reducing a multigroup problem to a one-group problem, using in the latter cross-sections that have been averaged over the spectrum, is not uncommon in reactor physics. It seems that this approach is workable, provided one can accept an underestimation of δ_3 of up to 2 per cent. The DATAPREP-II code has been based on this approach. However, before this code could be used for design calcula-

tions two more sources of error had to be introduced. Firstly, the evaluation of $\bar{T}$ in the one-group picture was still too lengthy and instead AMCLA was used to solve the flux ratios in the three regions. This increased the uncertainty of the δ_3-values which, for the lattices considered in this work, remained still below 2 per cent. Secondly, the spectrum needed for computing the average cross-sections from Eq. (42) was assumed to be spatially flat. This means that, as an additional approximation, the flux was taken to be separable in space and energy:

$$\Phi(\mathbf{r}, E) = c\varphi(\mathbf{r})\psi(E) \tag{44}$$

with the normalisation constant $c = 1 \Big/ \int_0^{E^*} \mathrm{d}E\psi(E)$.

In this approximation the expression for the effective $\overline{\Sigma}$'s becomes

$$\overline{\Sigma}_{s,t}(\mathbf{r}) = c \int_0^{E^*} \mathrm{d}E\, \Sigma_{s,t}(\mathbf{r}, E)\, \psi(E) \tag{45}$$

The integral equation from which the flux spectrum $\psi(E)$ can be solved was found by integration of Eq. (1) over all space and division by $c \int \mathrm{d}\mathbf{r}\, \varphi(\mathbf{r})$. This gave

$$\tilde{\Sigma}_t(E)\, \psi(E) = \int_0^{E^*} \mathrm{d}E'\, \tilde{\Sigma}_s(E' \to E)\, \psi(E') + \tilde{S}(E) \tag{46}$$

where use was made of the property Eq. (7) that, irrespective of the energy, the transport kernel integrates to unity, and with

$$\tilde{S}(E) = \int \mathrm{d}\mathbf{r}\, S(\mathbf{r}, E) \Big/ c \int \mathrm{d}\mathbf{r}\, \varphi(\mathbf{r}) \tag{47}$$

$$\tilde{\Sigma}_t(E) = \int \mathrm{d}\mathbf{r}\, \Sigma_t(\mathbf{r}, E)\, \varphi(\mathbf{r}) \Big/ \int \mathrm{d}\mathbf{r}\, \varphi(\mathbf{r}) \tag{48}$$

$$\tilde{\Sigma}_s(E' \to E) = \int \mathrm{d}\mathbf{r}\, \Sigma_s(\mathbf{r}, E' \to E)\, \varphi(\mathbf{r}) \Big/ \int \mathrm{d}\mathbf{r}\, \varphi(\mathbf{r}) \tag{49}$$

It is seen that the cross-sections with tilde are weighted with the spatial flux, i.e., with the flux ratios. Since no spatial dependence occurs in Eq. (46), it can be rapidly solved in the multigroup approach.

Thus, in the thermal calculations of DATAPREP-II, the integral transport equation (1) has been split into an equation for the spatial flux and one for the flux spectrum. The former, Eq. (39), is not solved directly but instead by AMCLA. The latter, Eq. (46), is solved by a multigroup technique with usually 20 equidistant speed groups (up to 40 groups may be taken, while 0.911 eV is the maximum cut-off). These two equations are coupled by their average cross-sections, Eqs. (45), (48), and (49). An iterative procedure has been used to solve them: firstly, an AMCLA calculation is done with Maxwellian averaged $\overline{\Sigma}_a$-values and 2200 m/s $\overline{\Sigma}_s$-values. The flux ratios

that are then obtained are used to construct $\tilde{\Sigma}_a$ and $\tilde{\Sigma}_s$ according to Eqs. (48) and (49). These $\tilde{\Sigma}$-values enter the multigroup spectrum calculation Eq. (46), which yields $\psi(E)$ over which the cross-sections are averaged to give new $\overline{\Sigma}$'s. This process is repeated two more times and terminated by a fourth AMCLA calculation of the flux ratios. Its convergence is extremely good and in all cases studied the g-factors and flux ratios were converged to an accuracy of better than 10^{-5}.

Only the BSJ and the WW scattering model have been built into the code. The spectrum produced by DATAPREP-II is not very sensitive to the choice of scattering model which can be understood as follows. Although the WW model has the largest average energy transfer per collision, its scattering cross-section, and thereby the frequency of the scattering collisions, is less than in the BSJ model (Table 1, Fig. 1). These two effects tend to cancel out so that almost the same spectrum is obtained from either model. The scattering cross-sections generated by the two models have meanwhile not been used to compute the average $\overline{\Sigma}_s$ from Eq. (45). This value was rather calculated by averaging of the scattering cross-sections read in from the library tape. Thereby, the difference in the two models is not even felt in AMCLA's flux ratios. The results quoted in this work have all been obtained with the BSJ model.

H_2O, D_2O, and O are the only moderators that can be treated by DATAPREP-II. Of these, only the latter may be present elsewhere than in the moderator region. Therefore the calculation of $\tilde{\Sigma}_s(E' \to E)$ only has to be done once, namely, with the flux ratios during iteration do not then affect the contribution of the moderator to $\tilde{\Sigma}_s(E' \to E)$, while the contribution from oxygen present in other regions is of marginal influence and will not be accounted for. The source term is, as usual, computed from a spatially flat $1/E$ epithermal flux. The scattering cross-sections used by AMCLA are transport-corrected, using for H_2O and D_2O the Radkowsky prescription [24].

DATAPREP-II has been written in FORTRAN 3600 for the CDC 3600 of the Kjeller Computer Installation, Norway. It uses an old version of AMCLA, where the first collision probability P_{21} is calculated by a double integration instead of evaluation of P_{11} direct from its analytical formula, Eqs. (38). The running time of 3 seconds for a case with 20 groups is therefore unnecessarily long. For more details reference should be made to the Kjeller Report [11].

4.4. Multigroup flux-ratio approach: the SATAN code

An obvious drawback of the method discussed in the preceding section is the assumption of a spatially constant spectrum which, at best, represents some average for the whole cell. Consequently, irrespective of whether DATAPREP-II produces correct flux ratios or not, it fails to do so with the regionwise variation of the spectrum-averaging g-factors, Eq. (21). Although the use of inaccurate g-factors will not be seriously felt in criticality calculations, where they appear as a ratio in the thermal

utilisation factor according to Eq. (20), they are necessary for a proper cell homogenisation. In burn-up studies, for example, it is essential to know at which rate the fissile nuclei are consumed or created and therefore the g-factors are, like the flux ratios, of fundamental importance to reactor design.

The method that will be described below has been developed to produce also accurate g-factors for the three regions: fuel, canning and moderator. The starting point was again the integral transport equation (1), which was integrated over the cell volume V. Making use of the property Eq. (7) that, at any energy, the transport kernel integrates to unity, the following equation was obtained

$$\hat{\Sigma}_t(E)\,\psi(E) = \int_0^{E^*} \mathrm{d}E'\,\hat{\Sigma}_s(E' \to E)\,\psi(E') + \hat{S}(E) \tag{50}$$

where $\psi(E)$ and $\hat{S}(E)$ are the volume-averaged cell spectrum and source, respectively, while the $\hat{\Sigma}$'s are flux-and-volume weighted cross-sections, i.e.,

$$\psi(E) = \frac{1}{V}\int \mathrm{d}\mathbf{r}\,\Phi(\mathbf{r}, E) = \sum_i \frac{V_i}{V} F_i(E)\,\psi(E) \tag{51}$$

$$\hat{S}(E) = \frac{1}{V}\int \mathrm{d}\mathbf{r}\,S(\mathbf{r}, E) = \sum_i \frac{V_i}{V} S_i(E) \tag{52}$$

$$\hat{\Sigma}_t(E) = \frac{1}{V\psi(E)} \int \mathrm{d}\mathbf{r}\,\Sigma_t(\mathbf{r}, E)\,\Phi(\mathbf{r}, E) = \sum_i \frac{V_i}{V} F_i(E)\,\Sigma_{t,i}(E) \tag{53}$$

$$\hat{\Sigma}_s(E' \to E) = \frac{1}{V\psi(E')} \int \mathrm{d}\mathbf{r}\,\Sigma_s(\mathbf{r}, E' \to E)\,\Phi(\mathbf{r}, E') = \sum_i \frac{V_i}{V} F_i(E')\,\Sigma_{s,i}(E' \to E) \tag{54}$$

with $F_i(E)$ being the ratio of the flux in region i to that of the whole cell (at energy E)

$$F_i(E) = \psi_i(E)/\psi(E) \tag{55}$$

and $\psi_i(E)$ as given by Eq. (22). In these equations the cell composition has been taken as being regionwise constant. The solution of the problem then proceeds in two steps. First, spatial calculations are done to generate the flux ratios $F_i(E)$ at a number of energy levels (groups). Next, these ratios are used to weight the cross-sections that enter the homogeneous-medium spectrum equation (50), which is solved in the multigroup approach. From the thus found cell spectrum $\psi(E)$, and the flux ratios at the different energies, the average spectrum per region is known as

$$\psi_i(E) = F_i(E)\,\psi(E) \tag{56}$$

The cell homogenisation can then be carried out because the thermal-group constants, i.e., the flux ratios and the g-factors, can be constructed from $\psi_i(E)$ according to Eqs. (24) and (22).

So far the multigroup flux-ratio approach is exact within the framework of the K-7 THERMOS approximations. It has a twofold advantage over the earlier discussed one-group method with effective cross-sections. Firstly, the present method can produce different spectra from one cell region to another so that the g-factors can take into account the spatial variation of the neutron spectrum. Secondly, the approximation of $\overline{T}$, Eq. (43), by computing it in a one-group picture using average values of Σ_t, has been avoided. It should be observed though, that a direct evaluation of the flux ratios $F_i(E)$ would need a two-dimensional transport kernel array for each energy group, the calculation of which would be equally lengthy as in K-7 THERMOS.

The fast code SATAN has been based on the principles outlined above. It makes use of AMCLA to compute the flux ratios $F_i(E)$ in the different energy groups, thereby avoiding the time-consuming direct solution of these ratios with the aid of transport kernels. The code has been written in ALGOL for the El X-8 computer at the Reactor Centrum Nederland, Petten (NH), the Netherlands [39], and in FORTRAN IV for the GE-625 computer at ASEA, Västerås, Sweden. The ALGOL version has been registered as number E 132 at the ENEA Computer Programme Library. The code works with a fixed group division and four cut-offs are available, namely, 0.230, 0.405, 0.625, and 0.911 eV. Either the BSJ kernel will be calculated by the programme, or the KY kernel is read in from library tape. The transport correction is always applied. Its running time per case was about 30 seconds on the El X-8, which is roughly a factor ten faster than the multishell, multigroup code MICROFLUX [8] on the same machine. It should be remarked, however, that the calculation of the BSJ kernel was included here and that in AMCLA still a rather slow routine for calculating the Ki_3 function was used. On the GE-625 its running time is 1.5 seconds per case, that is 50–100 times faster than K-7 THERMOS on the same machine. In these calculations the KY kernel was read in from the library tape, while the Ki_3 functions in AMCLA were evaluated according to the method described in Appendix 2.

The decoupling of spatial and spectral calculations in the present method has seemingly been a simple matter and no iterative procedure like in DATAPREP-II had to be applied. However, there does exist such a coupling, namely through the source term in the one-group spatial calculations. The one-group equation that should be solved for each of the thermal groups looks like

$$\Sigma_t(\mathbf{r}, E)\,\Phi(\mathbf{r}, E) = \int \mathrm{d}\mathbf{r}'\, T(\mathbf{r}' \to \mathbf{r}, E)\,[\Sigma_s(\mathbf{r}', E)\,\Phi(\mathbf{r}', E) + S(\mathbf{r}', E) + \Delta S(\mathbf{r}', E)] \qquad (57)$$

where $S(\mathbf{r}, E)$ is the slowing-down source, which may be assumed flat in the moderator and zero in canning and fuel; $\Delta S(\mathbf{r}, E)$ is the source caused by the in- and out-scattering of neutrons from and into the other energy groups of the thermalisation range:

$$\Delta S(\mathbf{r}, E) = \int_0^{E^*} \mathrm{d}E'\,[\Sigma_s(\mathbf{r}, E' \to E)\,\Phi(\mathbf{r}, E') - \Sigma_s(\mathbf{r}, E \to E')\,\Phi(\mathbf{r}, E)] \qquad (58)$$

Group	Energy, eV	Lattice									
		1	2	3	4	5	6	7	8	9	10
1	0.00158	+8.8	+27.5	+10.7	+23.9	+35.6	+29.5	−1.1	+8.5	+5.0	+19.3
2	0.0124	+0.6	+ 3.5	− 0.4	+ 2.2	+ 4.8	+ 2.9	−2.4	−0.1	+1.4	+ 4.6
3	0.0279	+0.2	+ 0.6	− 1.3	− 0.6	+ 0.1	− 0.4	−1.9	−0.8	+0.7	+ 1.5
4	0.0428	−0.1	− 0.4	− 1.4	− 1.2	− 1.2	− 1.2	−1.6	−0.8	+0.6	+ 0.4
5	0.0608	+0.1	− 0.5	− 1.0	− 1.0	− 1.2	− 1.0	−1.0	−0.5	+0.5	− 0.3
6	0.0866	+0.1	− 0.7	− 0.7	− 1.0	− 1.4	− 1.0	−0.6	−0.3	+0.3	− 0.7
7	0.117	+0.2	− 0.5	− 0.4	− 0.6	− 0.9	− 0.6	−0.4	−0.2	+0.4	− 0.7
8	0.152	+0.2	− 0.2	− 0.2	− 0.2	− 0.4	− 0.4	−0.2	−0.0	+0.6	− 0.4
9	0.199	+0.4	+ 0.4	− 0.0	+ 0.2	+ 0.3	+ 0.1	−0.2	+0.1	+0.7	+ 0.5
10	0.252	+0.6	+ 1.1	+ 0.2	+ 0.6	+ 1.2	+ 0.5	−0.2	+0.2	+1.0	+ 2.0
11	0.301	−0.2	+ 0.3	− 0.9	− 0.4	+ 0.1	− 0.4	−0.9	−0.6	+1.1	+ 2.4
12	0.365	+1.9	+ 2.5	+ 2.1	+ 2.6	+ 3.1	+ 2.5	+1.5	+1.5	+1.1	+ 2.3

Table 5. Percentage deviation of AMCLA disadvantage factors δ_3 from the K-7 THERMOS values in each of the twelve energy groups of SATAN.

In AMCLA the total source, i.e., $S + \Delta S$, has been taken to be flat. Although this is a good approximation for the slowing-down source, this will not necessarily be true for the thermalisation operator source ΔS.

In a non-absorbing medium, the spectrum will be Maxwellian and, as a consequence of the detailed balance, Eq. (4), ΔS will be zero. In fact, the absorptions which cause the flux to deviate from a Maxwellian shape make that $\Delta S \neq 0$, while in a heterogeneous medium they also cause flux gradients and, hence, are responsible for the spatial variation of ΔS. The integral of $\Delta S(\mathbf{r}, E)$ over all energies $E \leq E^*$ will be zero owing to Eq. (3), and consequently at low energies, including the thermal peak, ΔS will be positive and at the higher energies negative. The following considerations may illustrate this point more deeply. In any volume element, the total source $S + \Delta S$ will be equal to the sum of absorption and outflow. At the higher energies the absorption is small and the fluxes are quite flat, which implies a small streaming term. Thus, at high energies $S + \Delta S$ must be small; its two terms are of opposite sign and tend to cancel out. Therefore, small spatial variations in ΔS create strong fluctuations in the total source. Here one pays for the assumption of a flat, epithermal flux to generate the slowing-down source. In reality, there will still be small spatial variations of the epithermal flux and a more conscientious evaluation of the slowing-down source should result in an almost flat total source at the high energy end of the thermalisation range. At low energies, both the flux gradient and the absorption are much more pronounced, which leads to a large total source, i.e., to a positive value for ΔS. In fact, ΔS becomes so large in the lowest groups that it determines there the behaviour of the total source.

The above remarks have been verified for all the lattices of Appendix 1 by studying of the behaviour of ΔS and the slowing-down source with the aid of K-7 THERMOS.

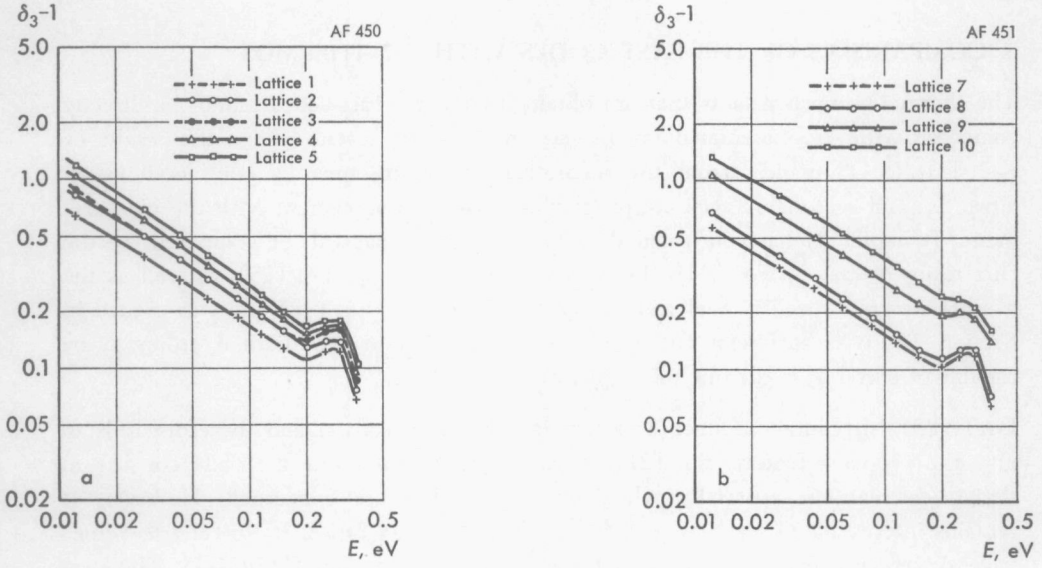

Fig. 10. Energy dependence of the disadvantage factor according to K-7 THERMOS.

It was furthermore observed that at the thermal peak the total source in lattice 10 varied by 15 per cent, while in the other lattices it was flat within 7 per cent. It is, however, difficult to draw quantitative conclusions from these considerations. Therefore, this point was further investigated by comparing AMCLA values for δ_3 in the 12 thermal groups with those obtained from K-7 THERMOS, where the energy exchange mechanism is taken into account. The results of this comparison are collected in Table 5; they are given as the percentage deviation of the AMCLA value from the K-7 THERMOS value. It is seen that the deviations are small for all groups but the lowest one. In the lowest group the cross-sections are large and the cell is very dense for the neutrons. In the K-7 THERMOS calculations the energy exchange processes will easily bring about a flattening of the neutron distribution. The influence of the lowest group on the final flux ratios is small and consequently this discrepancy will not be felt so strongly.

Another point that was noticed in this comparison is that the influence of the small U^{235} resonance at about 0.27 eV is well visible in most of the lattices. It is interesting that, with the exception of the well-moderated lattice 10, the energy exchange mechanism did not blur this effect (see Fig. 10). This indicates once more that the one-group transport effects predominate over the energy exchange process. It seems that one may feel safe in applying the flat source AMCLA calculations to generate the flux ratios per group $F_i(E)$. In power lattices, which are usually densely packed and where the moderator is thinner owing to the higher temperature and sometimes the voids, this approximation will certainly not be worse.

5. COMPARISON OF THE FAST CODES WITH K-7 THERMOS

The thermal-group constants that are obtained from the fast codes cannot be directly compared with experimental data. Instead, they will be tested against the results of K-7 THERMOS, which, from the theoretical viewpoint, may be considered as an advanced and reasonably accurate programme, while its agreement with the measurements (Chapter 3) has confirmed this. The quantities that will be compared are the flux ratios δ_2 and δ_3, Eq. (24), the density ratios ζ_2 and ζ_3, Eq. (25), as well as the average neutron speed in fuel and moderator, $\bar{v}_1$ and $\bar{v}_3$, Eq. (18). As was argued in Section 3.1, it is sufficient for a cell homogenisation in the thermal group to be capable of correctly predicting these quantities.

DATAPREP-II cannot produce a regionwise varying spectrum and therefore fails to give the proper g-factors, Eq. (21). This practically rules out the code for use in design calculations, especially when burn-up studies are concerned. However, it remains interesting to see how well it calculates the flux ratios. Its δ_2- and δ_3-values have therefore been compared with those obtained from K-7 THERMOS. The percentage deviation of the DATAPREP-II results are shown in Table 4. One of the two main assumptions in this code was the approximation of the "effective transport kernel" $\overline{T}$, Eq. (43), by a one-group calculation using spectrum-averaged values for the total scattering cross-section Σ_t. This approximation has already been discussed in Section 4.3, where it was found to decrease the flux ratios (see also Table 4). The other assumption was the use of a spatially flat spectrum for averaging the cross-sections that are needed in the one-group spatial calculations. This will generate some kind of cell-averaged spectrum, which, especially in loosely packed lattices, will lie too close to that of the moderator and which in all cases will be too soft in the fuel. The average absorption cross-section of the fuel therefore becomes too large, which leads to an increased contrast in the flux distribution, i.e., to increased flux ratios. It follows from Table 4 that this effect is stronger than that caused by the approximate

Lattice	δ_2[a]	δ_3	ζ_2[b]	ζ_3	$\bar{v}_1$[c]	$\bar{v}_3$
1	+0.2	+0.3	+0.3	+0.4	+0.1	0.0
2	+0.5	+0.4	+0.6	+1.2	+0.7	−0.2
3	−0.1	−0.7	−0.1	−0.6	+0.1	0.0
4	+0.5	−0.3	+0.5	+0.3	+0.4	−0.1
5	+0.7	+0.0	+0.5	+0.9	+0.8	−0.2
6	+0.4	−0.2	+0.4	+0.3	+0.5	−0.2
7	−1.5	−0.9	−1.6	−1.2	−0.1	+0.3
8	−0.7	−0.3	−0.8	−0.2	+0.1	0.0
9	−0.9	+1.2	−1.2	+1.3	−1.1	−1.2
10	−0.8	+0.9	−1.4	+1.8	+0.4	−0.4

[a] δ_i = ratio of average flux in region i to that in the fuel
[b] ζ_i = ratio of average neutron density in region i to that in the fuel
[c] $\bar{v}_i$ = average neutron speed in region i (1 = fuel, 2 = canning, 3 = moderator)

Table 6. Percentage deviation of some SATAN results from the K-7 THERMOS values in Table 2.

evaluation of $\bar{T}$. The net result is an overestimation of the flux ratios by DATAPREP-II, which increases with the lattice pitch. In power-reactor lattices, at operating conditions, the average spectrum will lie closer to that of the fuel, thus decreasing the positive error in the flux ratios so that they will be nearer to the proper values.

SATAN produces regionwise spectra as well as flux ratios and, hence, it gives all the information needed for a proper cell homogenisation. Its main approximation is the assumption of a flat source in the moderator for the calculation of the flux ratios per energy group. In spite of this decoupling of spatial and spectral calculations, the groupwise flux ratios $F_i(E)$ agreed well with those obtained from K-7 THERMOS, except for the lowest group and to a lesser degree for the highest group (see Table 5). In the lowest group this is due to the fact that there is a strong contact with the higher groups, where the neutron distribution is smoother. In the highest group the discrepancy is less and, of course, also caused by the decoupling of the spatial calculations from the spectral calculations. However, in the K-7 THERMOS calculations the net source in this group shows large variations owing to a small error in the slowing-down source, which was taken to be flat. At these energies the net source should be rather flat so that, physically speaking, the SATAN flux ratios in the highest group are probably better than the K-7 THERMOS ones. This error can be eliminated by the choice in the space-spectrum calculations of a cut-off energy which lies higher than that used to evaluate the thermal-group constants. This was done by the author and Tas [39] for the lattices 7 and 8. The cut-off in the spectrum calculations was 0.911 eV, while the group constants were computed below 0.405 eV. The effect on the spatial quantities ζ_2 and ζ_3 was less than -0.5 per cent, while the effect on the spectrum index was as much as $+1.9$ per cent in lattice 7 and $+1.2$ per cent in lattice 8. Of course, this effect is felt strongest in the hardness of the spectrum, which is more sensitive to the higher groups than the spatial distribution.

The final comparison of SATAN with K-7 THERMOS is presented in Tables 6 and 7. In Table 6 the percentage deviations of ζ, δ and $\bar{\nu}$ are listed for the ten lattices of Appendix 1. The K-7 THERMOS values for these quantities are given in Table 2. Although no measurements on regular power lattices were done, at least the SATAN

Fuel temp., °C ...	20		903		903		903	
Mod. temp., °C ...	20		285		285		285	
Void, % ...	0		0		30		60	
Quantity	K-7	Satan	K-7	Satan	K-7	Satan	K-7	Satan
δ_2	1.078	1.076	1.060	1.057	1.059	1.056	1.058	1.053
δ_3	1.161	1.157	1.115	1.114	1.109	1.110	1.101	1.108
ζ_2	1.106	1.105	1.080	1.075	1.080	1.074	1.079	1.072
ζ_3	1.224	1.221	1.156	1.154	1.148	1.147	1.138	1.142
$\bar{\nu}_1$	1.360	1.362	1.744	1.741	1.784	1.780	1.872	1.867
$\bar{\nu}_3$	1.291	1.290	1.682	1.681	1.723	1.723	1.812	1.811

Table 7. Comparison of SATAN with K-7 THERMOS for a power-reactor cell at room temperature and at different operating conditions.

results for such a lattice cell were compared with K-7 THERMOS. This cell is a typical example of the interior pins in the fuel assembly of the Oskarshamn BWR, a Swedish 400 MWe power reactor designed by ASEA and planned to be critical in 1970. It consists of a 2.0 per cent enriched UO_2 pin with a density of 10.25 g/cm^3 and a radius of 0.50 cm, canned in 0.08-cm-thick Zircaloy-2, and placed in a square H_2O-moderated cell of 1.63 cm pitch. The comparison was carried out for room temperature and for 285° C with 0, 30 and 60 per cent void in the coolant. In the hot case, the fuel temperature was taken to be 903° C. The results are given in Table 7. It follows from these comparisons that SATAN produces indeed thermal-group constants that agree well with the results from the more sophisticated and lengthier multishell, multigroup calculations.

6. CONCLUSIONS

The objective of this work was to develop and test a fast and accurate computational procedure for the thermal-group constants required for the cell homogenisation in design calculations. It turned out that the multigroup flux-ratio approach as embodied in SATAN produces, in single-pin lattices, results that closely agree with those from the more elaborate and time-consuming K-7 THERMOS. Consequently, SATAN, which combines calculational speed with accuracy, will be a powerful tool in the fuel-cycle studies for the design of light- and heavy-water reactors. The success of this approach is based on the relatively loose coupling between space and energy calculations, and on the accuracy of the group-wise flux ratios generated by AMCLA.

The experimental testing described in this work has been confined to the lattices of Appendix 1. Although they represent a rather wide range of lattice types, they do not cover typical power-reactor lattices at operating conditions nor lattices containing plutonium. For these types of lattice no intercell thermal-neutron distribution measurements have been reported in the open literature. Therefore, the reliability of K-7 THERMOS could only be tested in zero-energy lattices, where it was shown to be in good agreement with the results of careful measurements. In the IAEA Report [5] it has been shown that even for single-tube fuel elements this code agrees with the results of measured activation profiles. The good agreement of SATAN with K-7 THERMOS has thus only experimental back-up for the lattice types described in Appendix 1.

Meanwhile, as was pointed out several times in this work, there is no reason to believe that K-7 THERMOS should fail to predict accurately neutron distributions in power lattices. The investigations made on a regular lattice cell at high temperatures and with different void contents indicate that also for such power-lattice cells the agreement of SATAN with K-7 THERMOS is very satisfactory. Nevertheless, to

support fully the confidence in the applicability of these codes to regular lattices at high temperatures, with voids and with plutonium, additional intercell measurements in these types of reactor cell will be needed.

To sum up one may say:

SATAN calculations can replace K-7 THERMOS for regular single-pin lattices moderated by light and/or heavy water, including typical—but regular—power lattices. However, the reliability of the latter could only be tested against experiments performed on zero-energy lattice cells with uranium as the only fissile material. Since there does not seem to exist any indication that this code should fail in regular lattices at operating conditions, it is very likely that one may apply SATAN in the fuel-cycle studies of power-reactor design. One should keep in mind that these codes are probably not applicable to pin cells that lie in the vicinity of heterogeneities like control elements and water gaps. It remains a matter of further theoretical and experimental investigation to determine how such cells should be homogenised, i.e., how to obtain their group constants which will certainly be influenced by the heterogeneity.

ACKNOWLEDGEMENTS

The author would like to thank K. Bryhn-Ingebrigtsen, J. Smit, S. Takač, and A. Tas who made their experimental results available and with whom the author has had many discussions concerning their measuring techniques.

Thanks are due to T. Håvie for his helpful suggestions concerning numerical and programming techniques.

The author also feels indebted to Z. Weiss for valuable theoretical discussions.

The author is grateful to ASEA, Västerås, Sweden, who published this thesis.

APPENDIX 1. CHARACTERISTICS OF LATTICES STUDIED

The lattices that have been selected for testing and comparing of the theoretical methods were all three-region square or hexagonal lattices, moderated by H_2O, D_2O, or H_2O/D_2O. Although they cover a wide range of lattice types, they by no means represent all possible varieties. The main restriction is the fact that no power lattices at operating conditions—voids, high temperatures—could be included for testing the theoretical methods against measurements. This is due to the lack of experimental data on intercell neutron distributions in such lattices. The lattice characteristics are compiled in Table 8. The first six lattices are for the Norwegian zero-power assembly NORA [43]; the first two of them are so-called spectral shift lattices, where a mixture of light and heavy water is used as moderator. Lattices 7 and 8 are for the subcritical facility PUK [31], used for testing the Dutch ship-propulsion reactor design. They are the only two hexagonal lattices: the former consists of a regular array of fuel pins, while the latter is an open hexagonal lattice obtained from the former by introducing of a regular pattern of open fuel-rod positions. Lattices 9 and 10 are for the Yugoslavian zero-power RB reactor [44]. All the calculations and measurements on these lattices were done for room temperature (20° C) with the exception of lattice 6 where the temperature was raised to 60° C.

To have at least one comparison between the SATAN and K-7 THERMOS codes for a regular power lattice, a pin cell was taken that is representative of the 400 MWe BWR which is under construction near Oskarshamn, Sweden. This cell has been described in Chapter 5.

No.	Pitch	Shape	Fuel			Canning			Moderator % H_2O
			Enrichment %	Density g/cm³	Radius cm	Material	Density g/cm³	Radius cm	
1	2.31	sq.	UO_2—3.0	9.30	0.564	304—St. St.	8.03	0.635	45.0
2	3.66	sq.	UO_2—3.0	9.30	0.564	304—St. St.	8.03	0.635	45.0
3	1.90	sq.	UO_2—3.4	10.35	0.635	304—St. St.	8.03	0.690	100.0
4	2.31	sq.	UO_2—3.4	10.35	0.635	304—St. St.	8.03	0.690	100.0
5	2.69	sq.	UO_2—3.4	10.35	0.635	304—St. St.	8.03	0.690	100.0
6	2.31	sq.	——— as lattice 4, but at 60° C instead of 20° C ———						
7	1.51	hex.	UO_2—3.8	10.53	0.5	Al	2.58	0.6	100.0
8	1.85	hex.	UO_2—3.8	10.53	0.5	Al	2.58	0.6	100.0
9	8.0	sq.	U-nat.	18.8	1.25	Al	2.70	1.35	0.5
10	16.0	sq.	U-nat.	18.8	1.25	Al	2.70	1.35	0.5

Table 8. Characteristics of NORA lattices, Norway (Nos. 1—6), PUK lattices, the Netherlands (Nos. 7 and 8), and RB lattices, Yugoslavia (Nos. 9 and 10).

APPENDIX 2. CHEBYSHEV COEFFICIENTS FOR EVALUATING THE FUNCTIONS I_0, I_1, K_0 and Ki_3

The Bickley function $Ki_3(x)$ as well as the second-kind Bessel functions $I_0(x)$, $I_1(x)$ and $K_0(x)$, which together with $K_1(x)$ are all needed in AMCLA, have been calculated from their Chebyshev coefficients given in Tables 9 and 10. The Bessel function $K_1(x)$ was found from the relation

$$I_0(x)\,K_1(x) + I_1(x)\,K_0(x) = 1/x \tag{A 1}$$

Since especially a rapid calculation of $Ki_3(x)$ is essential for AMCLA, the x-range was divided into seven intervals $[a, b]$, chosen so that in each interval a few terms sufficed to give an absolute accuracy of better than 10^{-5}. In each of the intervals the Chebyshev representation is

$$Ki_3(x) = \sum_{r=0} c_r T_r(t) \tag{A 2}$$

with

$$t = (2x - b - a)/(b - a) \tag{A 3}$$

For the Bessel functions, the Chebyshev expansions are

$$I_0(x) = \sum_{r=0} c_r T_{2r}\left(\frac{x}{8}\right) \qquad (-8 \le x \le 8) \tag{A 4}$$

$$I_1(x) = \frac{x}{8} \sum_{r=0} c_r T_{2r}\left(\frac{x}{8}\right) \qquad (-8 \le x \le 8) \tag{A 5}$$

$$K_0(x) = \sum_{r=0} c_r T_{2r}\left(\frac{x}{8}\right) - \ln\left(\frac{x}{8}\right) I_0(x) \qquad (0 < x \le 8) \tag{A 6}$$

The summation over the even-order Chebyshev polynomials can be reduced to one of the type given in Eq. (A 2) by observing that

$$T_{2r}(t) = T_r(2t^2 - 1) \tag{A 7}$$

To evaluate a function from its Chebyshev coefficients, a procedure due to Clenshaw [20] was used. A sequence of constants d_{n-1}, d_{n-2}, ..., d_1, d_0 is computed from the recurrence relation

$$d_r = 2t d_{r+1} - d_{r+2} + c_r \qquad (d_n = d_{n+1} = 0) \tag{A 8}$$

r	$0.0 \le x \le 0.1$	$0.1 \le x \le 0.2$	$0.2 \le x \le 0.5$	$0.5 \le x \le 1.0$	$1.0 \le x \le 2.0$	$2.0 \le x \le 4.0$	$4.0 \le x \le 8.0$
1	0.785 398 16	0.785 231 79	0.784 900 31	0.779 899 3	0.767 050 75	0.654 502 7	0.280 440 9
2	−0.999 906	−0.994 716	−0.990 628 52	−0.953 726 8	−0.904 139 8	−0.645 332 4	−0.188 543 1
3	0.775 68	0.712 24	0.699 92	0.594 969 6	0.525 026 4	0.281 018 2	0.052 060 7
4	−0.710 4	−0.339 2	−0.360 177 78	−0.223 436 8	−0.184 307 2	−0.066 168 8	−0.007 327 1
5	0.896	—	0.109 037 04	0.040 140 8	0.037 644 8	0.008 260 8	0.000 522 65
6	—	—	—	—	−0.003 430 4	−0.000 430 4	−0.000 015 05

Table 9. Chebyshev coefficients a_r for $Ki_3(x)$.

The function value is then

$$f(x) = (d_0 - d_2)/2 \tag{A 9}$$

Another, faster, method was used to evaluate $Ki_3(x)$ from its Chebyshev coefficients. The polynomials $T_r(t)$ were replaced by their expression in powers of t and then rearranged to form

$$Ki_3(x) = \sum_{r=0} a_r t^r \tag{A 10}$$

Values for the various coefficients c_r and a_r are collected in Table 9 and 10, respectively. The coefficients for the Bessel functions were taken from Clenshaw [45].

r	$I_0(x)$ $\lvert x\rvert \leq 8$	$I_1(x)$ $\lvert x\rvert \leq 8$	$K_0(x)$ $0 < x \leq 8$
1	255.466 880	259.890 238	−21.057 660
2	190.494 320	181.312 616	− 4.563 434
3	82.489 033	69.395 918	8.005 369
4	22.274 819	16.334 551	5.283 633
5	4.011 674	2.571 460	1.511 536
6	0.509 493	0.287 856	0.259 084
7	0.047 719	0.023 993	0.030 081
8	0.003 416	0.001 543	0.002 536
9	0.000 192	0.000 079	0.000 163
10	0.000 009	0.000 003	0.000 003

Table 10. Chebyshev coefficients c_r for $I_0(x)$, $I_1(x)$ and $K_0(x)$.

REFERENCES

1. *H. C. Honeck,* Nucl. Sci. Eng. *18,* 49 (1964).
2. *Hiroshi Takahashi,* Nucl. Sci. Eng. *24,* 60 (1966).
3. *R. J. J. Stamm'ler,* K-7 THERMOS (Neutron thermalization in a heterogeneous cylindrically symmetric reactor cell), Kjeller Report KR-47 (1963).
4. *R. J. J. Stamm'ler,* The FORTRAN version of the neutron thermalization code K-7 THERMOS for the CDC 3600 computer, Kjeller Report KR-101 (1965).
5. *R. J. J. Stamm'ler, S. M. Takač, Z. J. Weiss,* Neutron thermalization in reactor lattice cells: An NPY-Project Report, Technical Reports Series No. 68, IAEA, Vienna (1966).[1]
6. *H. C. Honeck,* Nucl. Sci. Eng. *8,* 193 (1960).
7. *H. C. Honeck,* THERMOS, a thermalization transport theory code for reactor lattice calculations, BNL-5826 (1961).
8. *A. Tas, H. P. Struch, D. van Ligten,* Personal communication, RCN, Petten, Netherlands (1965).
9. *E. P. Wigner, J. E. Wilkins, Jr.,* Effect of temperature of the moderator on the velocity distribution of neutrons with numerical calculations for H as moderator, AECD-2275 (1944).
10. *H. J. Amster, R. Suarez,* The calculation of thermal constants averaged over a Wigner-Wilkins flux spectrum: Description of the SOFOCATE code, WAPD-TM-39 (1957).
11. *R. J. J. Stamm'ler, O. P. Tverbakk, Z. Weiss, J. M. Döderlein,* DATAPREP-II a reactor lattice homogenization and BIGG-II data preparation computer code, Kjeller Report KR-78 (1964).
12. *H. D. Brown, D. S. St. John,* Neutron energy spectrum in D_2O, DP-33 (1954).
13. *M. S. Nelkin,* Phys. Rev. *119,* 741 (1960).
14. *J. U. Koppel, J. A. Young,* Nucl. Sci. Eng. *19,* 412 (1964).
15. *H. C. Honeck,* Trans. Am. Nucl. Soc. *5,* 47 (1962).
16. *A. M. Weinberg, E. P. Wigner,* The physical theory of neutron chain reactors, The University of Chicago Press, pp. 336–340 (1958).
17. *P. Schofield,* The thermal neutron scattering law and neutron thermalization, BNL-770 (1962).
18. Integral neutron thermalization, Annual Summary Report, October 1, 1962–September 30, 1963, GA-4659 (1963).
19. *R. J. J. Stamm'ler,* K-7 TRANSPO (One-group neutron transport in a heterogeneous cylindrically symmetric reactor cell), Kjeller Report KR-71 (1964).
20. *T. M. Danielsen, T. Håvie, R. J. J. Stamm'ler,* On the numerical calculation of Bickley functions, Kjeller Report KR-55 (1963).
21. *I. Carlvik,* Proc. 3rd UN Int. Conf. PUAE, *2,* 225, Geneva (1964).
22. *D. A. Newmarch,* Errors due to the cylindrical cell approximation in lattice calculations, AEEW-R 34 (1960).
23. *H. C. Honeck,* Trans. Am. Nucl. Soc. *5,* 350 (1962).
24. *A. Radkowsky,* Temperature dependence of thermal transport mean free path, Physics Division Report for April, May, and June 1950, ANL-4476, pp. 89–101 (1950).
25. *J. A. Thie,* Nucl. Sci. Eng. *9,* 286 (1961).
26. *Z. Weiss, R. J. J. Stamm'ler,* Nucl. Sci. Eng. *19,* 374 (1964).
27. *I. Carlvik,* Calculations of neutron flux distributions by means of integral transport methods, AE-279, Stockholm, Sweden (1967).
28. *E. Andersen et al.,* Proc. 3rd UN Int. Conf. PUAE, *3,* 197, Geneva (1964).
29. *L. Adamski et al.,* Proc. 3rd UN Int. Conf. PUAE, *3,* 284, Geneva (1964).
30. *J. Smit,* Analysis of neutron spectra in UO_2 lattices moderated by mixtures of light and heavy water, using resonance detector foils, Kjeller Report KR-87 (1964).

31. *A. Tas, M. Bustraan,* The subcritical facility PUK, Experimental and critical experiments, Vol. I, IAEA, Vienna (1964).
32. *G. A. Price, R. L. Hellens,* Proc. 3rd UN Int. Conf. PUAE, *3,* 3, Geneva (1964).
33. *K. Bryhn-Ingebrigtsen,* Personal communication, IFA, Kjeller, Norway (1966).
34. *C. E. Wikdahl, F. Akerhielm,* Proc. 2nd UN Int. Conf. PUAE, *12,* 377, Geneva (1958).
35. *S. M. Takač, S. B. Krčevinac,* J. Nucl. Energy *21,* 233 (1967).
36. *T. Boševski, V. Spirić,* Experimental determination of the mean flux in the moderator of a square lattice cell, Boris Kidrič Institute Report IBK-171 (1965).
37. a) *J. Smit,* Measurement of the spatial variation of the thermal neutron energy spectrum in reactor cells, Kjeller Report KR-103 (1966).
    b) *J. Smit, R. J. J. Stamm'ler,* Nucl. Sci. Eng. *24,* 90 (1966).
38. *A. Amouyal, P. Benoist, J. Horowitz,* J. Nucl. Energy *6,* 79 (1957).
39. *R. J. J. Stamm'ler, A. Tas,* Theoretical and experimental determination of thermal-neutron group constants in regular lattices and a programme description of the code SATAN, RCN-62, Petten, Netherlands (1967).[1]
40. *Y. Fukai,* A comparison of some one-velocity transport approximations, BNL-669 (T-222) (1961).
41. *Z. Weiss,* Nucl. Sci. Eng. *22,* 60 (1965).
42. *K. M. Case, F. de Hoffman, G. Placzek,* Introduction to the theory of neutron diffusion, Washington, D.C., Government Printing Office, p. 33 (1954).
43. *E. Andersen et al.,* NORA, a zero power experimental reactor facility, Kjeller Report KR-41 (1963).
44. *D. Popović et al.,* Bull. of the Boris Kidrič Institute, *9,* 1 (1959).
45. *C. W. Clenshaw,* Chebyshev series for mathematical functions, Math. Tables, Vol. 5—National Physical Laboratory—London: Her Majesty's Stationery Office (1962).
46. *D. J. Hughes, R. B. Schwartz,* Neutron cross-sections, BNL-325, 2nd ed. (1958).

[1] References Nos. 5 and 39 together contain a fairly exhaustive description of the theoretical and experimental methods that are discussed in this thesis. In Reference No. 5 also other methods are described while more lattice types and measurements are analysed.

SUMMARY

The aim of the present thesis has been to develop and test rapid computational methods for producing thermal-neutron group constants in uniform single-pin lattices moderated by H_2O and/or D_2O. These constants enable homogenisation of the lattice cell with respect to the thermal-neutron distribution, because they provide sufficient information to describe its thermal reaction rates. Two examples of such fast codes are given: DATAPREP-II and SATAN. They are fast enough to be incorporated in calculational schemes for fuel-cycle studies and reactor design. The former replaces the thermalisation range with a single energy group, thereby reducing the problem to a one-group calculation of flux ratios using effective cross-sections. These cross-sections are averages over the cell spectrum, which has been assumed to be spatially independent. The latter calculates flux ratios for a number of energy groups and homogenises the cell by flux and volume averaging of the cross-sections per group. The average cell spectrum can then be evaluated from which, using also the flux ratios, the spectra per region and the thermal-group constants can be constructed. Here the main assumption is that the source is flat in each group, whereby the flux-ratio calculations in the groups have been decoupled from the energy-transfer calculations.

Experimental verification of these codes is not possible because the integral quantities they produce cannot be directly measured. Therefore the fast codes have been tested against the results of the sophisticated code K-7 THERMOS. This code evaluates the thermal-neutron distribution in space and energy in a circularised cell under the assumption of isotropic scattering in the laboratory system. With this code the various approximations that have been used are discussed and found to be satisfactory. However, the final check on the reliability of K-7 THERMOS as a standard for testing the fast codes should be made by a comparison of its results with measurements. Such a comparison has been carried out on a number of uniform uranium lattices at room temperature. Good agreement was observed in those cases where the experimental data were carefully analysed and the perturbing effects of the measuring device eliminated. The comparison could not be extended to plutonium lattices nor to uniform lattices in power reactors at operating temperatures and with voids, because accurate experimental data are still lacking. However, there does not seem to be any reason why K-7 THERMOS should fail for these types of lattice cell, since they do not offer new problems.

With the reliability of K-7 THERMOS thus established, it could be used to test the fast codes. SATAN appeared to be in good agreement, while neglecting the spatial variation of the spectrum in the lattice cell turned out to be a serious drawback for DATAPREP-II. Hence, the fast code SATAN, which generates thermal-group con-

stants with about the same accuracy as the more sophisticated and time-consuming calculations of K-7 THERMOS, becomes a valuable tool for fuel-cycle studies and nuclear-reactor design.

The studies reported here have been confined to regular lattice cells and neither K-7 THERMOS nor the other codes should be applied thoughtlessly to cells that lie in the vicinity of irregularities like control elements and water gaps. The interesting question how to calculate group constants for such cells falls outside the scope of this thesis.

SAMENVATTING

Het doel van dit proefschrift is het ontwikkelen en testen van snelle berekeningsmethoden voor het produceren van de groepskonstanten van thermische neutronen in regelmatige staafroosters gemodereerd met licht en/of zwaar water. Deze konstanten maken een homogenisatie van de roostercel mogelijk voor zover het de thermische neutronen betreft omdat ze voldoende informatie verschaffen om de thermische reaktiesnelheden te beschrijven. Twee voorbeelden van snelle kodes worden gegeven: DATAPREP-II en SATAN. Ze zijn snel genoeg om gebruikt te worden in de berekeningsschema's voor brandstofcyclus studies en reaktor ontwerp. In de eerste kode wordt het thermalisatiegebied door een enkele energie groep vervangen waardoor het probleem wordt teruggebracht tot een een-groeps berekening van flux verhoudingen met behulp van effektieve werkzame doorsneden. Deze werkzame doorsneden zijn gemiddelden over het cel spektrum welke als ruimtelijk onafhankelijk is aangenomen. De tweede kode berekent de flux verhoudingen voor een aantal energie groepen en homogeniseert de cel door de werkzame doorsneden per energie group te middelen over de flux en het volume. Het gemiddelde spektrum in de cel kan dan berekend worden. Daaruit worden de spektra per gebied en de thermische groepskonstanten gevonden onder gebruikmaking van de flux verhoudingen per groep. Hier is de belangrijkste veronderstelling dat de totale bronsterkte in elke groep vlak is waardoor de ruimtelijke berekeningen van de flux verhoudingen in de groepen losgekoppeld zijn van de spektrum berekeningen.

Een experimentele bevestiging van de betrouwbaarheid van deze kodes is niet mogelijk omdat de integrale grootheden die ze produceren niet rechtstreeks meetbaar zijn. Daarom werden de snelle kodes getest aan de resultaten van de meer verfijnde kode K-7 THERMOS. Deze kode berekent de verdeling van de thermische neutronen in ruimte en energie in een gecylindriseerde cel onder de aanname van isotrope verstrooiing in het laboratorium systeem. Met behulp van deze kode werden de diverse benaderingen welke gebruikt zijn besproken en voldoende bevonden. Een afdoende bevesti-

ging van de betrouwbaarheid van K-7 THERMOS als standaard kode om de snelle kodes aan te testen kan echter uitsluitend verschaft worden door zijn resultaten met metingen te vergelijken. Zo'n vergelijking is gedaan voor een aantal regelmatige uranium roosters bij kamertemperataur. Goede overeenstemming bestond in die gevallen waar de experimentele gegevens nauwkeurig waren geanalyseerd en waar de verstoringen veroorzaakt door de meting zelf waren geëlimineerd. Deze vergelijking kon niet worden gedaan voor plutonium roosters noch voor regelmatige roosters van energieproducerende kokend-water reaktoren in bedrijf omdat hiervoor nog steeds nauwkeurige meetgegevens ontbreken. Er schijnt echter geen reden te bestaan om te veronderstellen dat K-7 THERMOS zou falen voor dergelijke roosters aangezien ze geen nieuwe problemen bieden.

Nadat aldus de betrouwbaarheid van K-7 THERMOS was vastgesteld konden de snelle kodes er aan getest worden. SATAN bleek in goede overeenstemming te zijn, terwijl daarentegen in DATAPREP-II het verwaarlozen van de ruimtelijke variatie van het spektrum in de rooster cel een ernstig nadeel bleek te zijn. De snelle kode SATAN produceert dus thermische groepskonstanten die ongeveer even nauwkeurig zijn als die van de meer verfijnde en langdurige berekeningen van K-7 THERMOS. Daardoor wordt SATAN een waardevol onderdeel in brandstofcyclus berekeningen en in ontwerp studies van kernreaktoren.

De hier gerapporteerde onderzoekingen hebben zich beperkt tot regelmatige roosters en noch K-7 THERMOS noch de andere kodes mogen gedachteloos toegepast worden op rooster cellen die zich in de nabijheid van bijvoorbeeld kontrole elementen en waterspleten bevinden. De belangwekkende vraag hoe de groepskonstanten voor cellen in de nabijheid van zulk een onregelmatigheid in het rooster berekend moeten worden valt buiten het bestek van dit proefschrift.

STELLINGEN

1. Boyntons metingen in sterk ondergemodereerde staafroosters, waarmee hij een minimum in de „disadvantage factor" als funktie van de water:uranium verhouding aantoont, zijn niet beslissend. Dit minimum bestaat niet eens.
   Z. Weiss en *R. J. J. Stamm'ler*, Nucl. Sci. Eng. *19*, 374 (1964).
   A. R. Boynton, Nucl. Sci. Eng. *23*, 393 (1965).

2. Fukai's bewering, dat in integrale transport theorie de neutronen flux in een cylindrische cel met een isotroop reflekterende grens vlak zou zijn bij die grens, is onjuist.
   Y. Fukai, Nukleonik, *7*, 144 (1965).

3. De „disadvantage factor" in een normale pin cel, dat is de verhouding van de flux in de moderator tot die in de brandstof, neemt *toe* wanneer men de isotroop reflekterende celgrens vervangt door een volkomen absorbator.

4. De orientatiehoek van de dysprosium draden in Kleijns aktiveringmetingen in de hexagonale roostercellen van LEAD behoort 12°14′ te zijn in plaats van 15°.
   H. R. Kleijn, On the determination of microscopic reactor parameters using an exponential assembly, Thesis, Delft (1965).

5. De spektrum index gedefiniëerd in dit proefschrift behoort algemeen gebruikt te worden om het thermische neutronen spektrum te karakteriseren. Het is een veel geschiktere parameter hiervoor dan de gemiddelde snelheid van de thermische neutronen of hun „temperatuur".
   J. Smit en *R. J. J. Stamm'ler*, Nucl. Sci. Eng. *24*, 90 (1966).

6. Ondanks het Doppler effekt bestaat in een zwaar-water gemodereerde reaktor het gevaar dat de temperatuurs-koefficient van de brandstof positief wordt bij toenemende burnup. Dit is bij een licht-water gemodereerde reaktor uitgesloten.
   B. M. Townes et al., Calculation of reactivity coefficients for a BLW lattice cell, AECL-2649 (1966).

7. De diffusie koefficient in de nabijheid van een zwarte absorbator dient gemiddeld te worden over een spektrum dat zelfs zachter is dan het oneindig-medium spektrum.

8. In dynamische studies van een kokend-water reaktor met behulp van het punt-model wordt vaak ten onrechte het gebied waar onderkoeld koken optreedt niet expliciet behandeld. Dit is van grote invloed op de overdrachtsfunktie.
   J. A. Hodde, Control rod oscillation and transient pressure tests in the Big Rock Point boiling water reactor, GEAP-4448 (1966).

9. De bewering van Weinberg en Wigner dat „. . . more insight into the principal phenomena of neutron diffusion has been gained from the solution of the two-group equations than from the extensive and accurate solution of multigroup equations by means of large computing machines", is tegenwoordig niet meer juist.
   A. M. Weinberg en *E. P. Wigner,* The physical theory of neutron chain reactors, The University of Chicago Press, p. 513 (1959).

10. Wanneer men in een BWR brandstof patroon de individuele pincellen homogeniseert dan dient dit te geschieden ten opzichte van de flux aan de rand van de cel en niet, zoals men zou verwachten, ten opzichte van de gemiddelde flux in de cel.

11. Algoritme 91, „Chebyshev Curve-Fit" van Albert-Newhouse, gepubliceerd in Communications of the ACM, 5, 281 (1962) bevat fouten en is bovendien inefficient zowel wat betreft geheugenplaatsen als rekentijd.

12. Hoewel de theorieën van Freud, Jung en Adler in hun uitgangspunten mogen verschillen is het sukses van hun respektieve behandelingsmethoden gebaseerd op een algemeen principe waarschijnlijk door geen van drieën ooit vermoed.

13. Het koningsgambiet is een geschikte opening voor simultaanspelers.
   Dr. M. Euwe, Theorie der Schaakopeningen, No. 12, G. B. van Goor Zonen's Uitg. mij. N.V. (1956).

Proefschrift: R. J. J. Stamm'ler
Västerås, 13 maart, 1968